Supporting Information

Regioselectivity of hyoscyamine 6β-hydroxylase-catalysed hydroxylation as revealed by high-resolution structural information and QM/MM calculations

Anna Kluza[1,#], Zuzanna Wojdyla[1,#], Beata Mrugala[1], Katarzyna Kurpiewska[1,2], Przemyslaw J. Porebski[1,3], Ewa Niedzialkowska[1,3], Wladek Minor[3], Manfred S. Weiss[4], Tomasz Borowski[1]

***1 - Jerzy Haber Institute of Catalysis and Surface Chemistry**, Polish Academy of Sciences, Niezapominajek 8, PL-30239 Krakow, Poland*
***2 - Department of Crystal Chemistry and Crystal Physics,** Faculty of Chemistry, Jagiellonian University, Gronostajowa 2, PL-30387 Krakow, Poland*
***3 - Department of Molecular Physiology and Biological Physics,** University of Virginia, 1340 Jefferson Park Avenue Pinn Hall, Charlottesville, VA 22908, USA*
***4 - Macromolecular Crystallography,** Helmholtz-Zentrum Berlin für Materialien und Energie, Albert-Einstein-Str. 15, D-12489, Berlin, Germany*

***Correspondence to Tomasz Borowski:** Jerzy Haber Institute of Catalysis and Surface Chemistry, Polish Academy of Sciences, Niezapominajek 8, PL-30239 Krakow, Poland. ncborows@cyf-kr.edu.pl.*

#These authors contributed equally to this work

ATGGCGACCCTGGTGAGCAACTGGAGCACCAACAACGTTAGCGAGAGCTTCATCGCGCCGCTGGAGAAGC
GTGCGGAAAAAGACGTGGCGCTGGGTAACGATGTTCCGATCATTGACCTGCAGCAAGATCACCTGCTGATC
GTGCAGCAAATTACCAAGGCGTGCCAGGACTTCGGTCTGTTTCAAGTGATTAACCACGGCGTTCCGGAGAA
GCTGATGGTGGAGGCGATGGAAGTTTATAAAGAATTCTTTGCGCTGCCGGCGGAGGAAAAGGAGAAATTCC
AGCCGAAGGGCGAACCGGCGAAATTTGAGCTGCCGCTGGAACAAAAGGCGAAACTGTACGTGGAGGGTGA
ACGTCGTTGCAACGAGGAATTCCTGTATTGGAAGGACACCCTGGCGCATGGTTGCTACCCGCTGCACGAGG
AACTGCTGAACAGCTGGCCGGAGAAACCGCCGACCTACCGTGATGTTATCGCGAAGTATAGCGTGGAAGTT
CGTAAACTGACCATGCGTATCCTGGACTATATTTGCGAGGGTCTGGGCCTGAAACTGGGTTACTTTGATAAC
GAACTGACCCAGATTCAAATGCTGCTGGCGAACTACTATCCGAGCTGCCCGGACCCGAGCACCACCATTGG
TAGCGGTGGCCACTACGACGGCAACCTGATTACCCTGCTGCAGCAAGATCTGGTGGGCCTGCAGCAACTGA
TCGTTAAGGACGATAAATGGATCGCGGTGGAGCCGATTCCGACCGCGTTCGTGGTTAACCTGGGTCTGACC
CTGAAGGTTATGAGCAACGAGAAATTTGAAGGCAGCATCCACCGTGTGGTTACCCACCCGATTCGTAACCGT
ATCAGCATTGGTACCCTGATCGGCCCGGACTATAGCTGCACCATCGAGCCGATTAAGGAACTGATTAGCCA
GGAAAACCCGCCGCTGTACAAACCGTACCCGTATGCGGAGTTCGCGGAAATCTACCTGAGCGATAAGAGCG
ACTATGATGCGGGTGTTAAGCCGTACAAAATTAACCAGTTTCCGAAC

Figure S1. DNA sequence of H6H from *Datura metel*, codon-optimized for expression in *Escherichia coli*. Nucleotides that were later removed in truncated form of H6H are indicated in green.

Table S1. Primers used for H6H truncation in the LIC protocol.

	Primer DNA sequence	T_m
Forward	TACTTCCAATCCAATGCCGATGTTCCGATCATTGACCTG	66.6°C
Reverse	TTATCCACTTCCAATGTTATCAGTTCGGAAACTGGTTAATTTTGTACG	65.4°C

Table S2. Crystallization details.

H6H:ligand	PDB ID	Protein sample	Mother liquor
H6H:NOG:Hyo	6TTM	20 mg/ml H6H in water 100 mM N-oxalylglycine 10 mM hyoscyamine	100 m M strontium chloride 180 mM sodium formate 21% PEG 3350
tH6H:NOG:Hyo	6TTN	29 mg/ml tH6H in water 100 mM N-oxalylglycine 10 mM hyoscyamine	100 mM strontium chloride 200 mM sodium formate 20% PEG 3350
tH6H:2OG	6TTO	37.5 mg/ml tH6H in water	100 mM disodium 2-oxoglutarate 100 mM strontium chloride 200 mM sodium formate 25% PEG 3350

Table S3. Data collection statistics for metals identification in tH6H.

H6H:ligand	tH6H:NOG:Hyo			
Data collection				
Beamline	BL14.1 BESSY II	BL14.1 BESSY II	BL14.1 BESSY II	BL14.1 BESSY II
Detector	Pilatus 6M	Pilatus 6M	Pilatus 6M	Pilatus 6M
No. of frames	3600	3600	3600	3600
Exposure time / frame [s]	0.1	0.1	0.1	0.1
Energy [keV]	7.05	7.25	8.24	8.44
Wavelength [Å]	1.7586	1.7101	1.5047	1.4690
Space group	$P2_12_12_1$	$P2_12_12_1$	$P2_12_12_1$	$P2_12_12_1$
α = β = γ [°]	90	90	90	90
a, b, c [Å]	39.94 79.83 104.74	39.83 79.61 104.55	39.82 79.93 104.77	39.84 80.07 104.87
Resolution [Å]	43.79-1.86 (1.97-1.86)	43.7-1.79 (1.90-1.79)	43.81-1.53 (1.63-1.53)	43.87-1.55 (1.65-1.55)
R_{meas}[%]	7.7 (22.8)	7.2 (15.7)	6.6 (37.7)	11.7 (83.5)
I / σ (I)	17.57 (5.85)	19.47 (8.36)	16.69 (3.61)	10.12 (1.46)
CC(1/2)	99.7 (96.4)	99.7 (98.0)	99.9 (90.0)	99.6 (73.1)
Completeness [%]	99.0 (95.4)	99.1 (95.8)	99.2 (95.5)	99.0 (95.1)
Multiplicity	6.13 (4.50)	6.15 (4.45)	6.05 (4.50)	6.09 (4.72)
B(Wilson) [A²]	23.14	23.91	23.57	25.69
Mosaicity	0.089	0.073	0.148	0.140

Table S4. Difference map peaks analysis in metal identification. The theoretical ratio values were estimated with crossec implemented in CCP4i [1,2]. Experimental ratios were calculated with five sulfurs from cysteine and methionine residues with the highest peak values.

Energy [keV]	Dataset	Peak values in anomalous difference maps [rmsd]						
			Crystal contact			Active center		
		S	Sr	Observed ratio Sr/S	Estimated ratio	Ni	Observed ratio Ni/S	Estimated ratio Ni/S
7.05	tH6H:NOG:Hyo	11.16	39.64	3.55	3.23	9.95	0.89	0.91
7.25	tH6H:NOG:Hyo	14.34	47.41	3.31	3.24	12.49	0.87	0.91
8.24	tH6H:NOG:Hyo	12.54	43.81	3.49	3.28	12.2	0.97	0.92
8.44	tH6H:NOG:Hyo	6.92	22.79	3.29	3.29	63.9	9.23	7.48

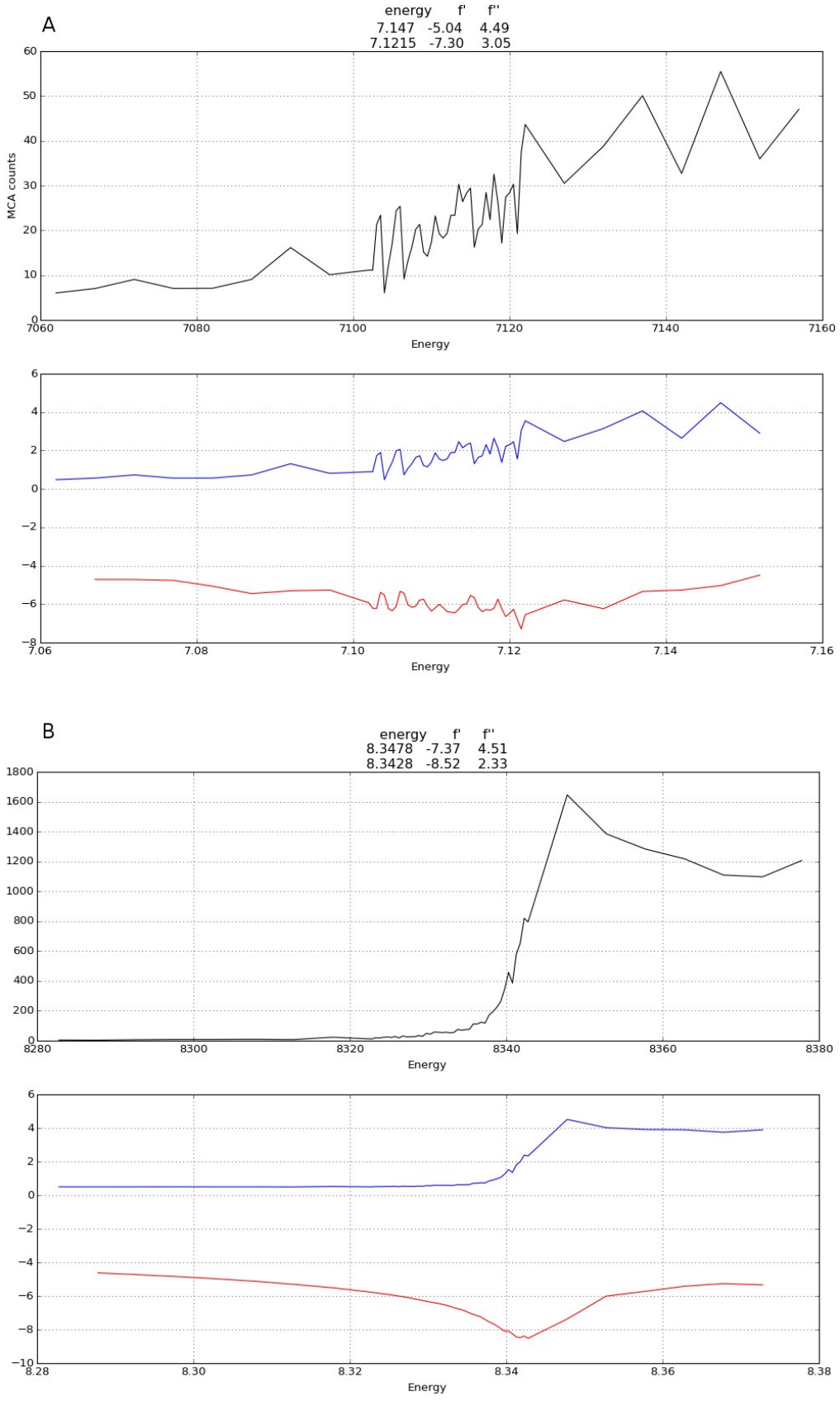

Figure S2. X-ray energy scans in the vicinity of (A) Fe (7.062 keV - 7.152 keV) and (B) Ni (8.283 keV - 8.373 keV) absorption K-edges performed for tH6H:NOG:Hyo crystals.

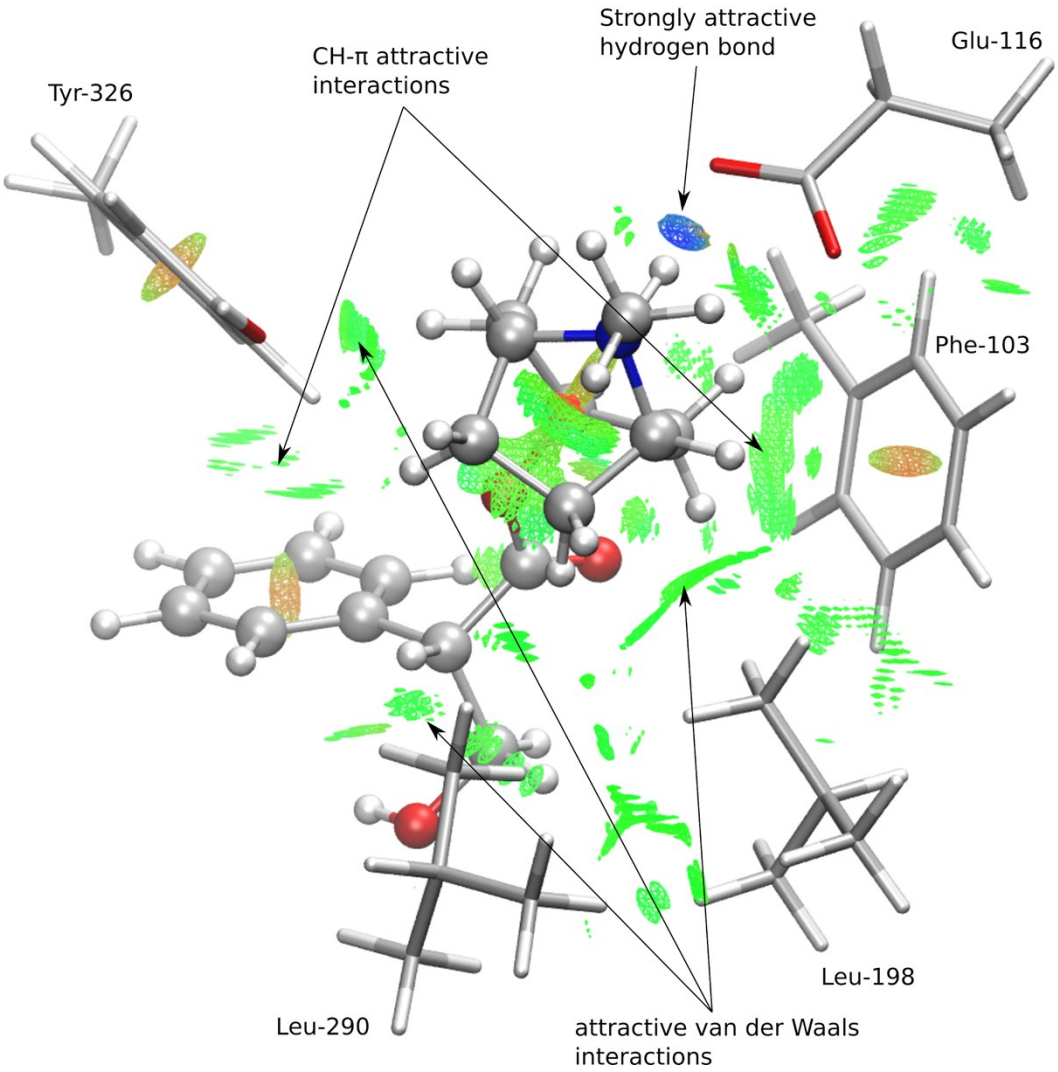

Figure S3. Interactions of hyoscyamine with most prominent residues in the binding pocket, as revealed by NCI analysis [3] performed with the NCIPLOT program [4].

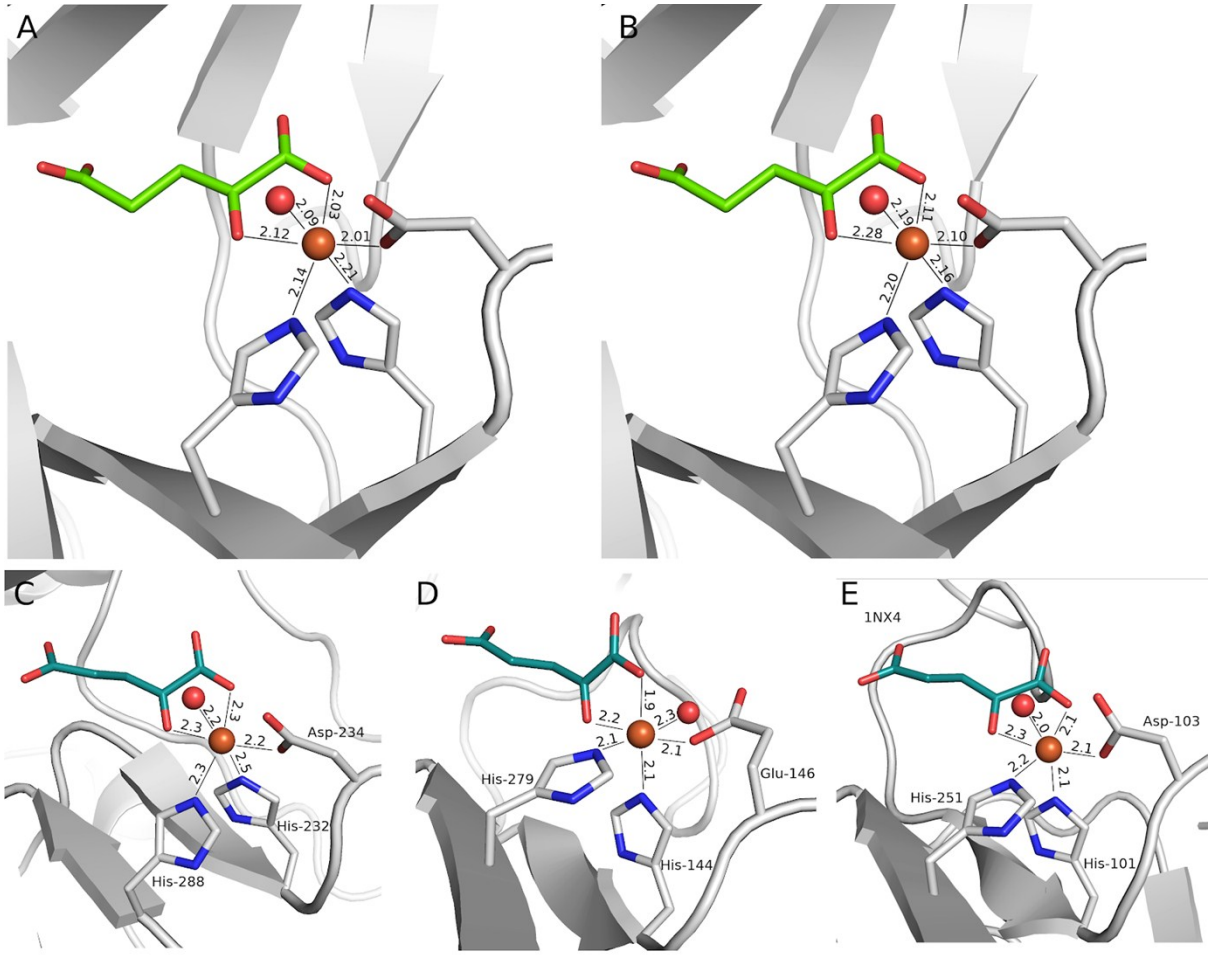

Figure S4. Active site of (A) representative structure of the dominant cluster for MD simulations for tH6H:2OG:hyoscyamine complex, (B) QM/MM optimised tH6H:2OG:hyoscyamine complex, (C) X-ray structure for anthocyanidin synthase (PDB ID: 1GP5 [5]), (D) X-ray structure for clavaminic acid synthase (PDB ID: 1DRY [6]) and (E) carbapenem synthase (PDB ID: 1NX4 [7]).

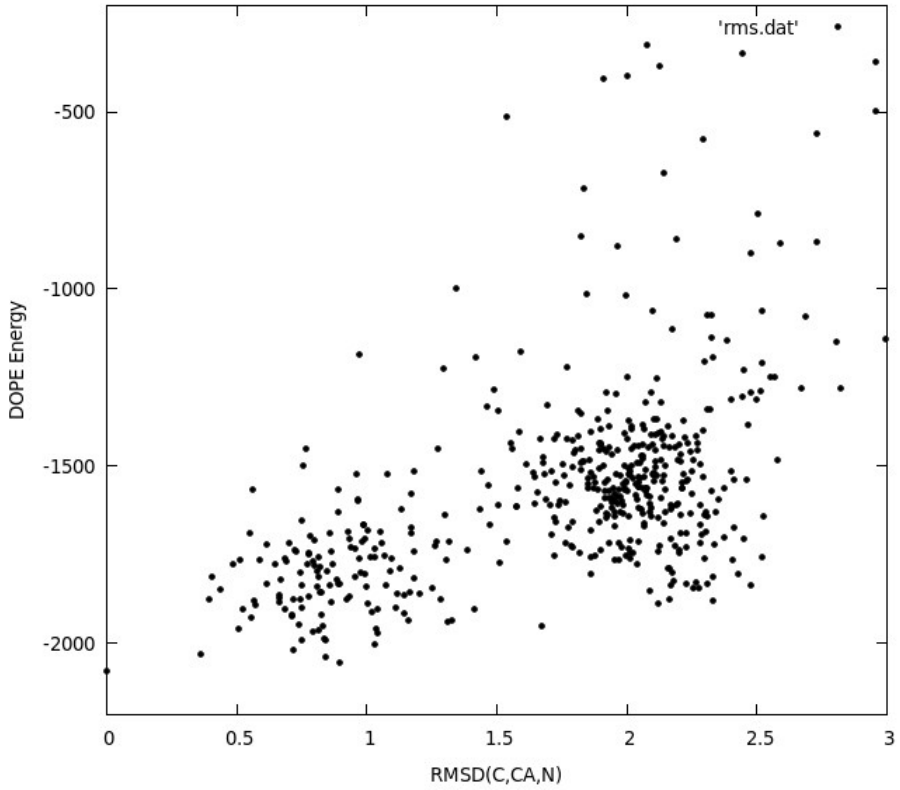

Figure S-C1. DOPE energy of the conformations from 500 independent optimizations of loops (residues: 117-128 and 206-215) plotted as a function of the RMSD error.

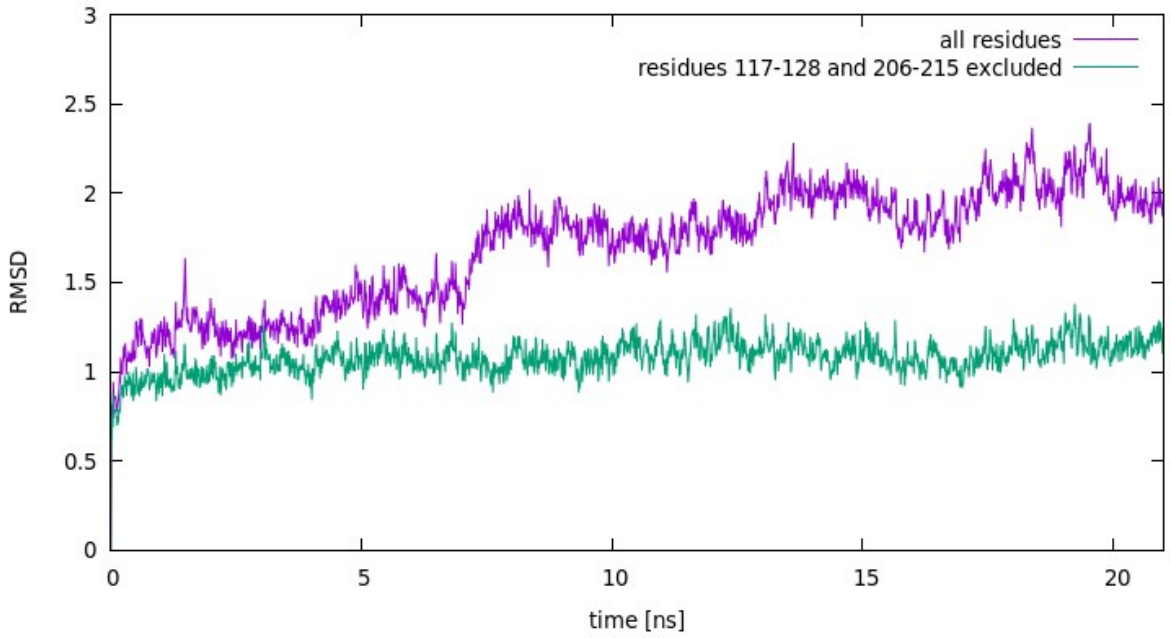

Figure S-C2. RMSD vs time plot for tH6H:2OG:hyoscyamine complex. Excluding the loop regions (residues: 117-128 and 206-215) from analysis lowers the RMSD of the system.

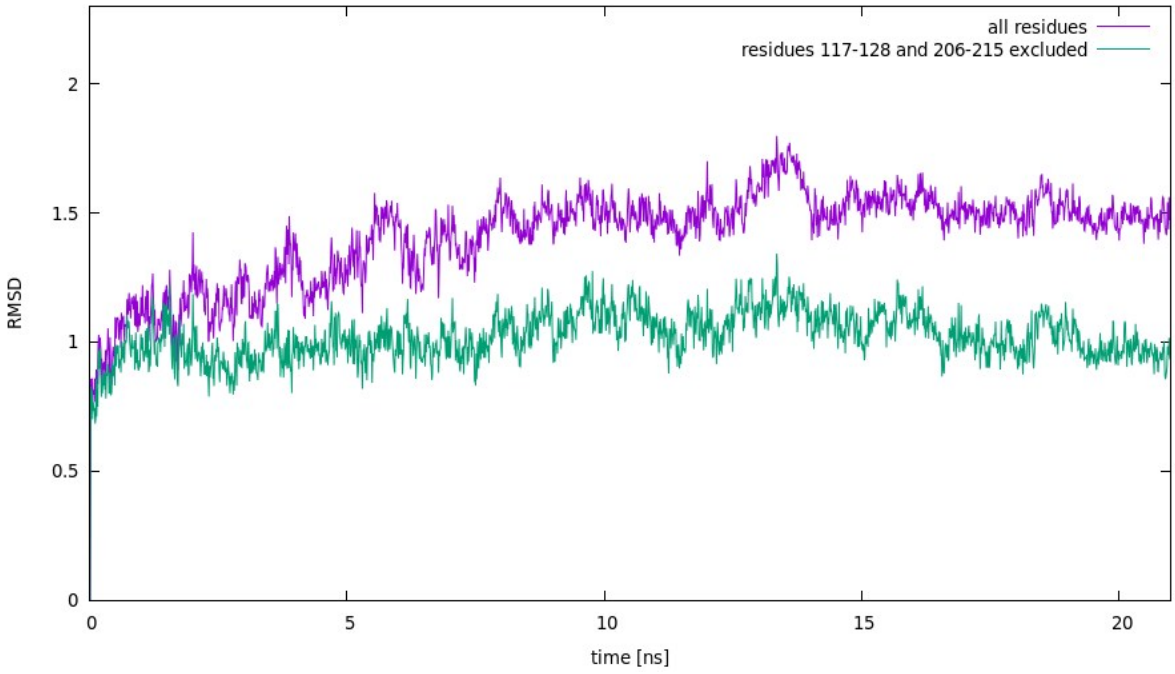

Figure S-C3. RMSD vs time plot for tH6H:succinate:hyoscyamine complex. Excluding the loop regions (residues: 117-128 and 206-215) from analysis lowers the RMSD of the system.

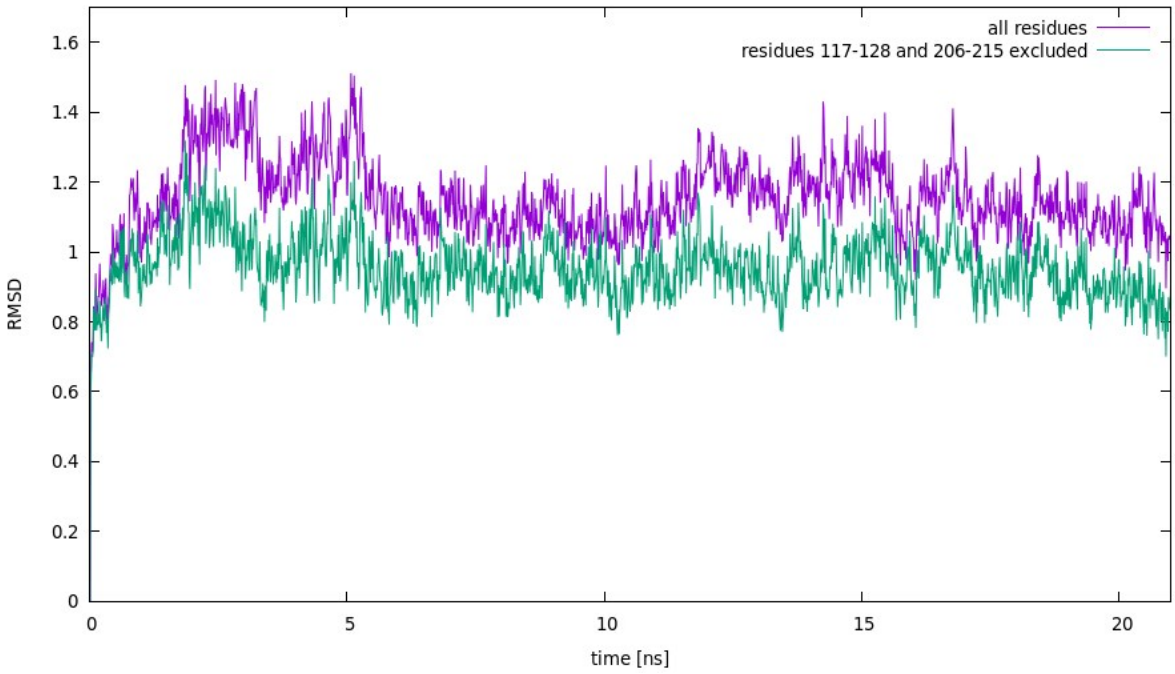

Figure S-C4. RMSD vs time plot for tH6H:succinate:hyoscyamine complex. Excluding the loop regions (residues: 117-128 and 206-215) from analysis lowers the RMSD of the system.

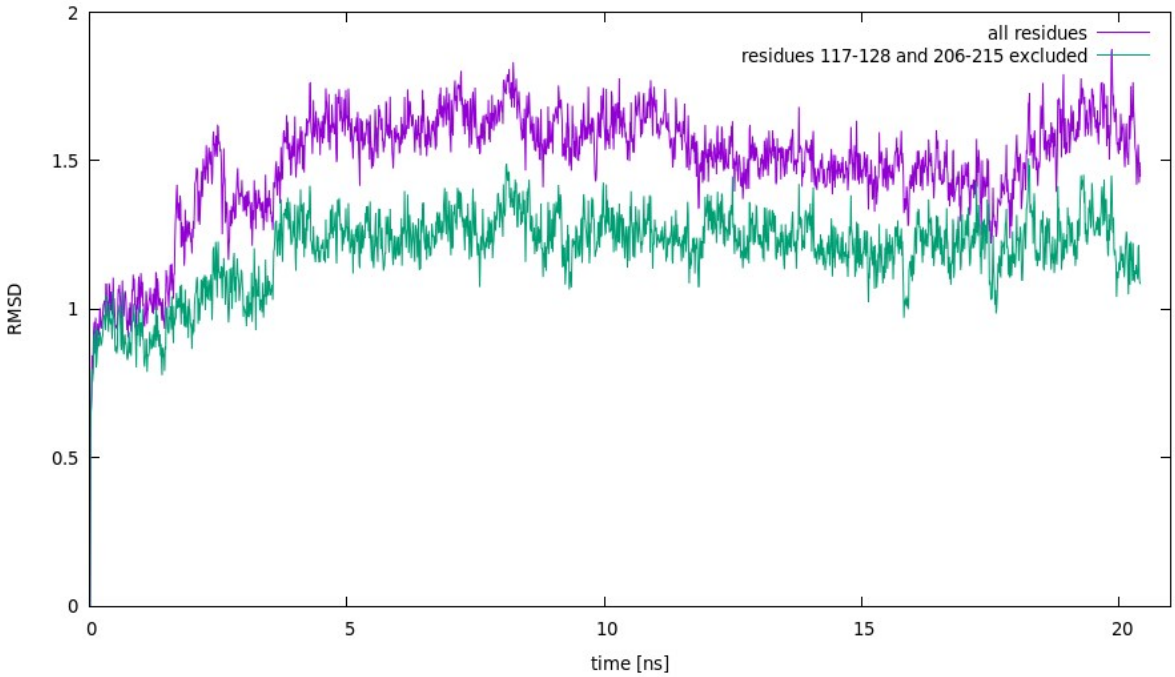

Figure S-C5. RMSD vs time plot for tH6H:succinate:hyoscyamine complex. Excluding the loop regions (residues: 117-128 and 206-215) from analysis lowers the RMSD of the system.

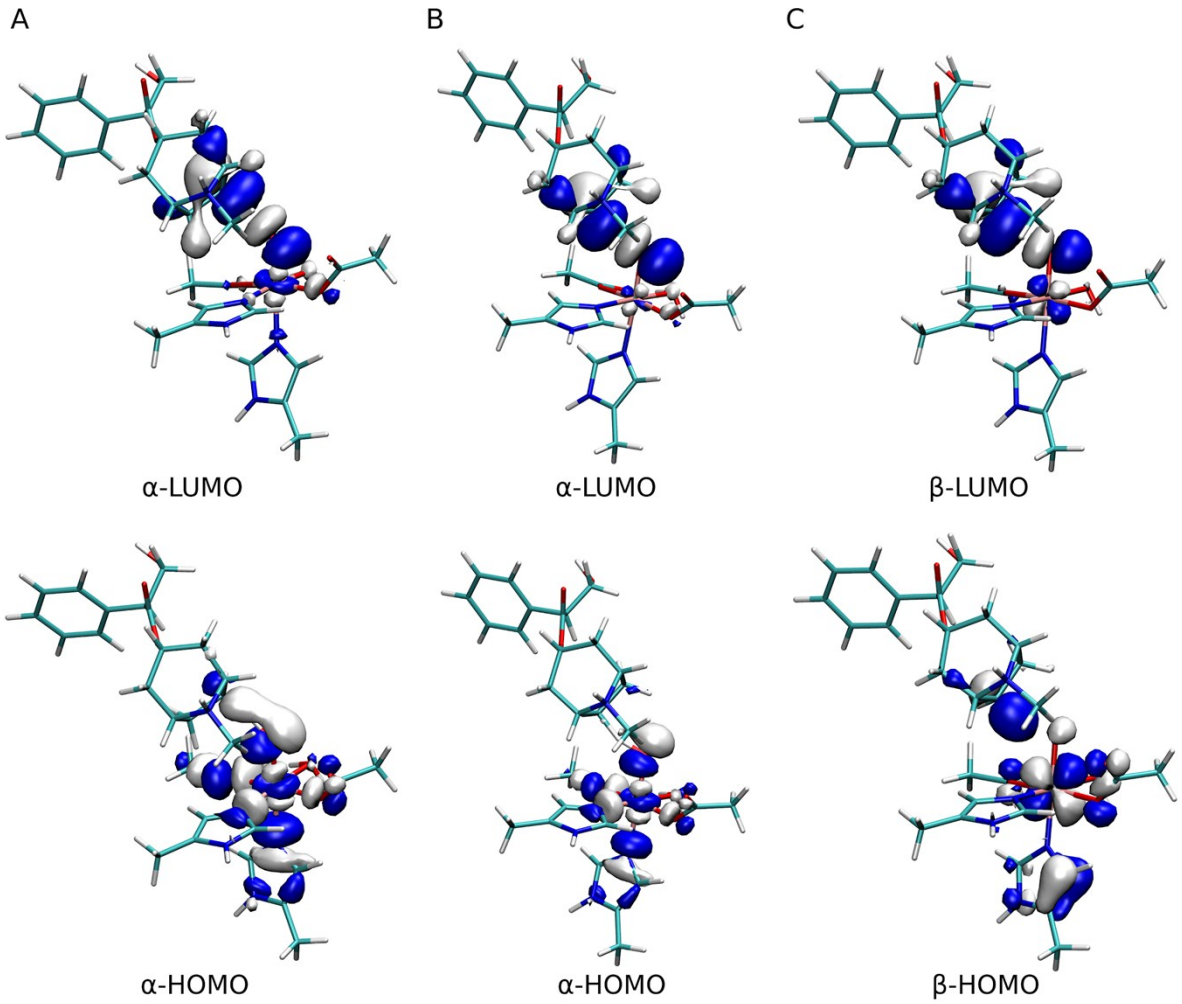

Figure S-C5. The HOMO and LUMO orbitals for (A) $\mathbf{TS_{HAT1\text{-}C6}}$,(B) $\mathbf{TS_{HAT1\text{-}C7}}$ and (C) $\mathbf{TS'_{HAT1\text{-}C7}}$.

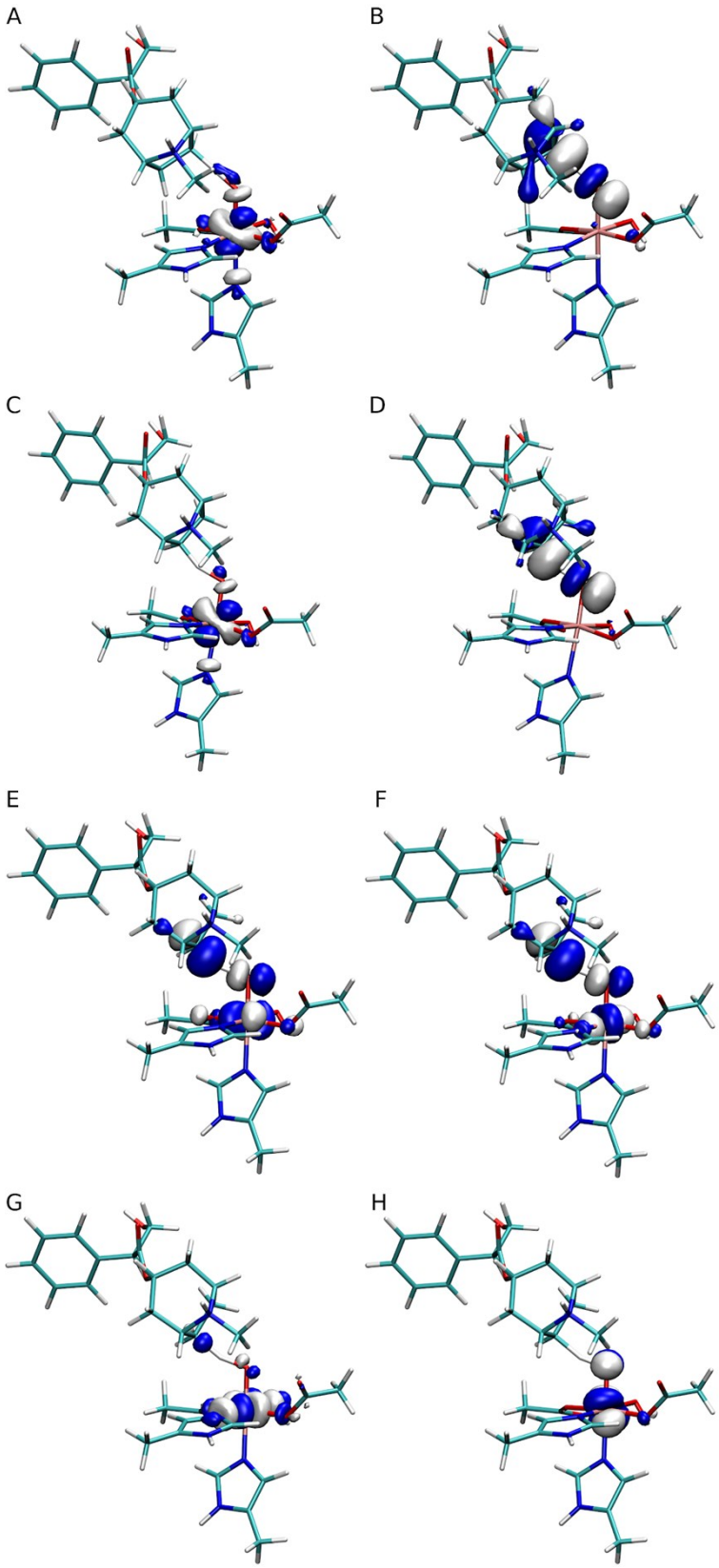

Figure S-C6. Contours of the key natural orbitals for spin density: with positive eigenvalue (α-spin) (A) and negative eigenvalue (β-spin) (B) for $\mathbf{TS}_{\mathbf{HAT1\text{-}C6}}$; with positive eigenvalue (α-spin) (C) and negative eigenvalue (β-spin) (D) for $\mathbf{TS}_{\mathbf{HAT1\text{-}C7}}$ and with positive eigenvalue (α-spin) (E, F, G and H) for $\mathbf{TS'}_{\mathbf{HAT1\text{-}C7}}$.

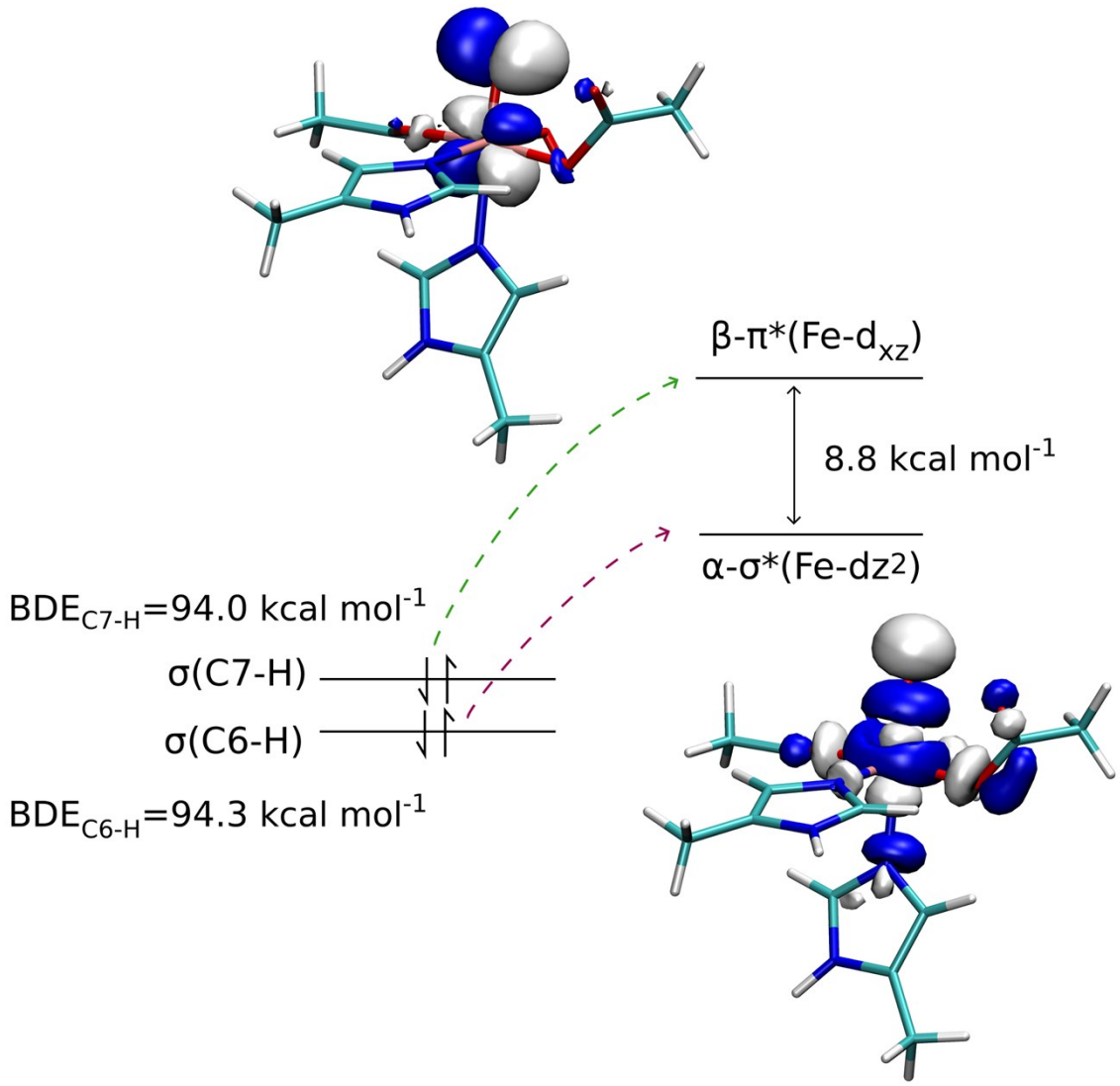

Figure S-C7. Energy scheme for the orbitals of hyoscyamine that donate the electron and the electron accepting orbitals of oxoferryl. The green arrow corresponds to transition in $\mathbf{TS_{HAT1\text{-}C6}}$ and the purple one to $\mathbf{TS'_{HAT1\text{-}C7}}$. Conceptually, in $\mathbf{TS_{HAT1\text{-}C7}}$ α electron from the σ(C7-H) orbital is accepted by a mixture of analogous α orbitals of oxoferryl.

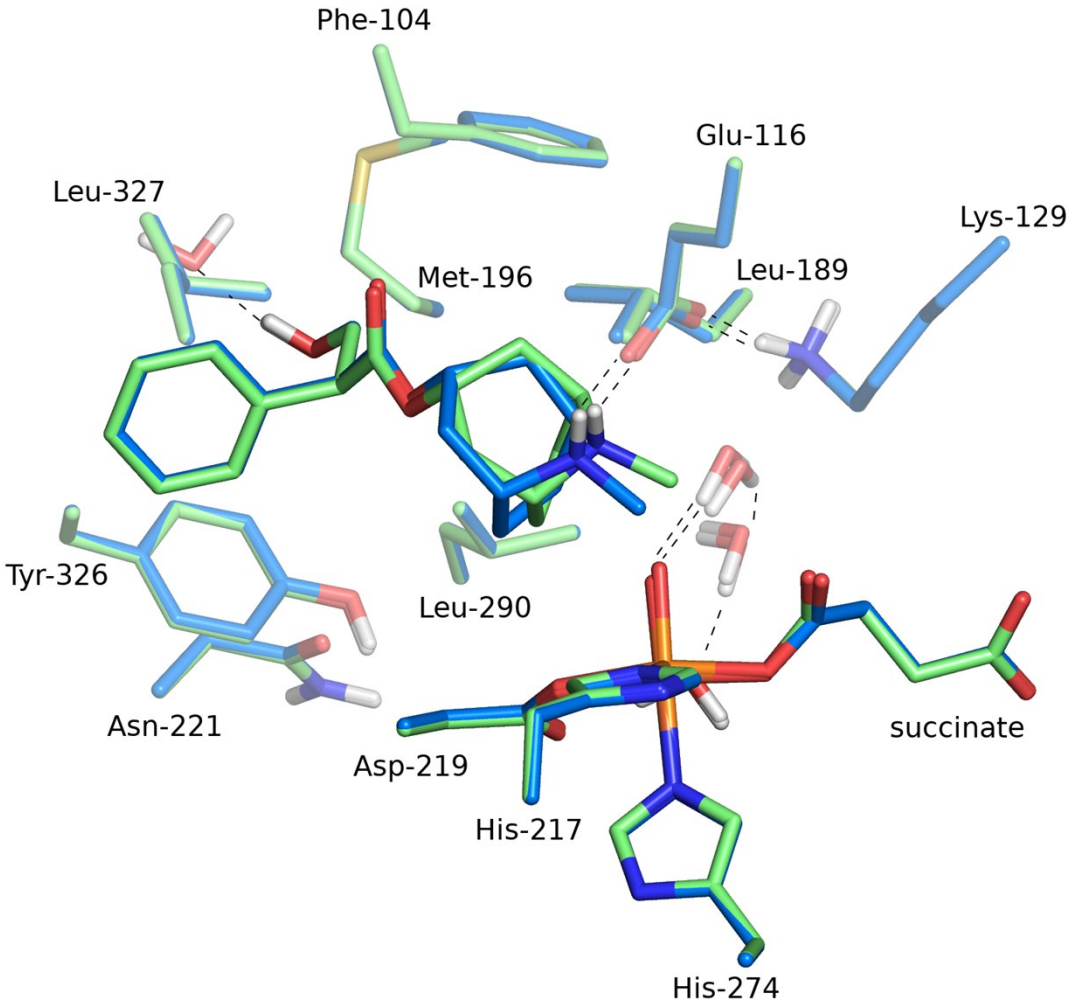

Figure S-C8. Superimposed optimised structures for $\mathbf{TS_{HAT1\text{-}C6}}$ (blue) $\mathbf{TS_{HAT1\text{-}C7}}$ (light green).

Table S-C1. The ONIOM energy barriers (ΔE) for tH6H variants of $\mathbf{TS_{HAT1\text{-}C6}}$ and $\mathbf{TS_{HAT1\text{-}C7}}$ lacking single amino acid side chains. The change in barrier caused by the removal of the side chain is given as ΔΔE. Coulomb, van der Waals and bonded contributions are reported as $\Delta\Delta E^{Coulomb}$, $\Delta\Delta E^{vdW}$ and $\Delta\Delta E^{bond}$, respectively. Values are given in kcal mol^{-1}.

	$\mathbf{TS_{HAT1\text{-}C6}}$					$\mathbf{TS_{HAT1\text{-}C7}}$				
residue	ΔE	ΔΔE	$\Delta\Delta E^{Coulomb}$	$\Delta\Delta E^{vdW}$	$\Delta\Delta E^{bond}$	ΔE	ΔΔE	$\Delta\Delta E^{Coulomb}$	$\Delta\Delta E^{vdW}$	$\Delta\Delta E^{bond}$
none (wt)	13.39	0.00	0.00	0.00	0.00	24.03	0.00	0.00	0.00	0.00
Phe-103	13.07	0.32	0.16	0.17	0.00	24.18	-0.15	-0.29	0.14	-0.01
Leu-105	13.33	0.06	0.05	0.00	0.00	23.94	0.08	0.05	0.04	0.00
Leu-107	13.21	0.18	0.07	0.10	0.00	23.86	0.17	0.09	0.07	0.01
Glu-116	15.50	-2.12	-2.33	0.22	-0.01	28.31	-4.28	-4.71	0.64	-0.21
Lys-129	13.70	-0.31	-0.61	0.33	-0.03	20.89	3.13	3.75	-0.77	0.15
Thr-131	13.26	0.13	0.02	0.11	0.00	24.00	0.03	-0.24	0.24	0.03
Ala-133	13.32	0.06	0.01	0.05	0.01	23.84	0.19	0.01	0.17	0.01
Ile-194	13.37	0.01	0.04	-0.01	-0.02	23.97	0.05	0.06	0.00	-0.01
Met-196	13.28	0.10	0.09	0.01	0.00	23.80	0.23	0.30	0.11	-0.17
Leu-198	13.17	0.21	-0.01	0.25	-0.02	23.51	0.52	0.13	0.43	-0.04
Asn-200	13.56	-0.18	-0.17	0.04	-0.05	23.78	0.25	0.51	-0.15	-0.11
Tyr-202	13.42	-0.03	-0.13	0.18	-0.08	24.09	-0.06	-0.33	0.30	-0.03
Asn-221	13.49	-0.10	-0.25	0.18	-0.03	24.01	0.01	-0.08	0.13	-0.04
Thr-224	13.67	-0.29	-0.50	0.25	-0.04	24.65	-0.62	-1.01	0.39	0.01
Leu-226	13.35	0.04	-0.08	0.12	0.00	23.98	0.05	-0.04	0.09	0.00
Leu-233	13.46	-0.07	-0.12	0.10	-0.05	24.07	-0.05	-0.09	0.09	-0.04
Asn-256	13.28	0.11	0.19	-0.20	0.12	24.33	-0.30	-0.36	0.05	0.01
Thr-260	13.42	-0.04	-0.15	0.09	0.02	24.10	-0.07	-0.28	0.17	0.04
Val-276	13.55	-0.17	-0.09	-0.08	0.01	24.08	-0.05	-0.08	0.02	0.01
Leu-290	13.10	0.29	0.03	0.24	0.01	23.80	0.23	0.03	0.12	0.08
Tyr-295	13.35	0.04	0.09	-0.06	0.00	24.02	0.01	0.11	-0.10	0.00
Tyr-319	13.43	-0.04	-0.07	-0.01	0.03	24.11	-0.09	-0.06	-0.04	0.01
Ala-320	13.39	0.00	0.00	0.00	0.00	24.03	0.00	0.00	0.00	0.00
Phe-322	13.36	0.02	0.08	-0.05	-0.01	23.98	0.05	0.14	-0.09	0.00
Ala-323	13.42	-0.03	-0.01	-0.03	0.00	24.02	0.01	0.00	0.01	0.00
Glu-324	14.00	-0.61	-0.62	0.01	0.00	24.59	-0.56	-0.56	0.00	0.00
Tyr-326	13.88	-0.49	-0.64	0.09	0.06	23.68	0.35	-0.86	1.31	-0.11
Leu-327	13.18	0.21	0.15	0.03	0.03	23.42	0.61	0.09	0.56	-0.03
Lys-330	11.52	1.86	1.93	-0.05	-0.01	23.73	0.30	0.40	-0.13	0.03
WAT-365	13.23	0.16	0.07	0.09	-0.01	23.74	0.29	-0.02	0.31	0.00
WAT-370	14.03	-0.65	-0.63	-0.02	0.00	24.57	-0.55	-0.49	-0.06	0.01
WAT-372	13.30	0.08	0.09	0.00	0.00	23.91	0.12	0.14	-0.02	-0.01
WAT-375	13.54	-0.16	-0.34	0.16	0.02	24.27	-0.24	-0.64	0.37	0.04
WAT-442	13.20	0.18	0.22	-0.03	-0.01	23.82	0.21	0.29	-0.08	0.00
WAT-605	13.16	0.23	-0.12	0.35	0.00	24.06	-0.04	-0.41	0.36	0.01
water-1	16.72	-3.33	**-6.02**	2.35	0.35	24.38	-0.35	**-0.98**	0.56	0.07
WAT-782	13.53	-0.14	-0.12	-0.02	0.00	23.95	0.08	0.14	-0.05	-0.01

WAT-2175	13.18	0.20	0.30	-0.09	-0.01	23.59	0.43	0.47	-0.01	-0.02
WAT-3097	12.91	0.48	0.51	0.00	-0.03	23.69	0.34	0.26	0.09	-0.01
WAT-3155	13.37	0.01	0.01	0.00	0.00	24.03	-0.01	0.20	-0.20	-0.01
WAT-4290	13.39	0.00	0.01	-0.01	0.00	23.82	0.21	0.28	-0.05	-0.02
WAT-4432	13.24	0.14	0.20	-0.04	-0.01	24.00	0.02	0.13	-0.09	-0.01
WAT-4451	13.32	0.06	0.18	-0.10	-0.01	23.96	0.06	0.14	-0.06	-0.01
WAT-4521	13.42	-0.03	-0.02	-0.01	0.00	24.17	-0.15	-0.15	0.00	0.00
WAT-5452	13.38	0.01	0.10	-0.10	0.00	24.19	-0.16	-0.16	-0.01	0.01
WAT-5484	13.40	-0.02	0.09	-0.10	0.00	24.07	-0.04	-0.03	-0.02	0.00
WAT-5548	13.34	0.04	-0.09	0.11	0.01	23.67	0.35	0.47	-0.10	-0.02
WAT-5765	12.97	0.42	0.56	-0.14	-0.01	23.76	0.27	0.71	-0.34	-0.10
WAT-6529	13.40	-0.02	0.02	-0.04	0.00	24.02	0.01	-0.02	0.03	0.00
WAT-7051	14.10	-0.71	-0.64	-0.10	0.03	24.16	-0.13	-0.09	-0.05	0.01
WAT-7395	13.82	-0.43	0.01	-0.45	0.01	24.27	-0.24	-0.23	-0.01	0.00
WAT-8073	13.59	-0.21	-0.17	-0.06	0.03	23.92	0.11	0.26	-0.14	0.00
WAT-9161	14.34	-0.96	-1.60	0.55	0.09	25.01	-0.98	-1.64	0.58	0.08
WAT-9453	13.35	0.03	-0.20	0.22	0.01	24.19	-0.17	-0.65	0.46	0.03
WAT-9464	13.16	0.23	0.22	0.02	-0.01	23.96	0.06	0.11	-0.03	-0.01
WAT-9501	13.62	-0.24	-0.11	-0.14	0.01	24.02	0.01	0.25	-0.24	0.00
WAT-9665	13.38	0.00	0.23	-0.22	-0.01	23.88	0.15	0.40	-0.24	-0.01
WAT-11739	13.53	-0.14	-0.08	-0.06	0.00	23.94	0.08	0.08	0.01	0.00
WAT-12117	13.39	0.00	0.00	0.00	0.00	24.02	0.00	0.00	0.00	0.00
sum over AA		-0.85	-2.87	2.10	-0.08		0.04	-3.34	3.80	-0.42
sum over waters		-4.75	-7.31	2.12	0.44		-0.22	-1.2	0.96	0.02
TOTAL		-5.60	-10.18	4.22	0.37		-0.17	-4.54	4.76	-0.40

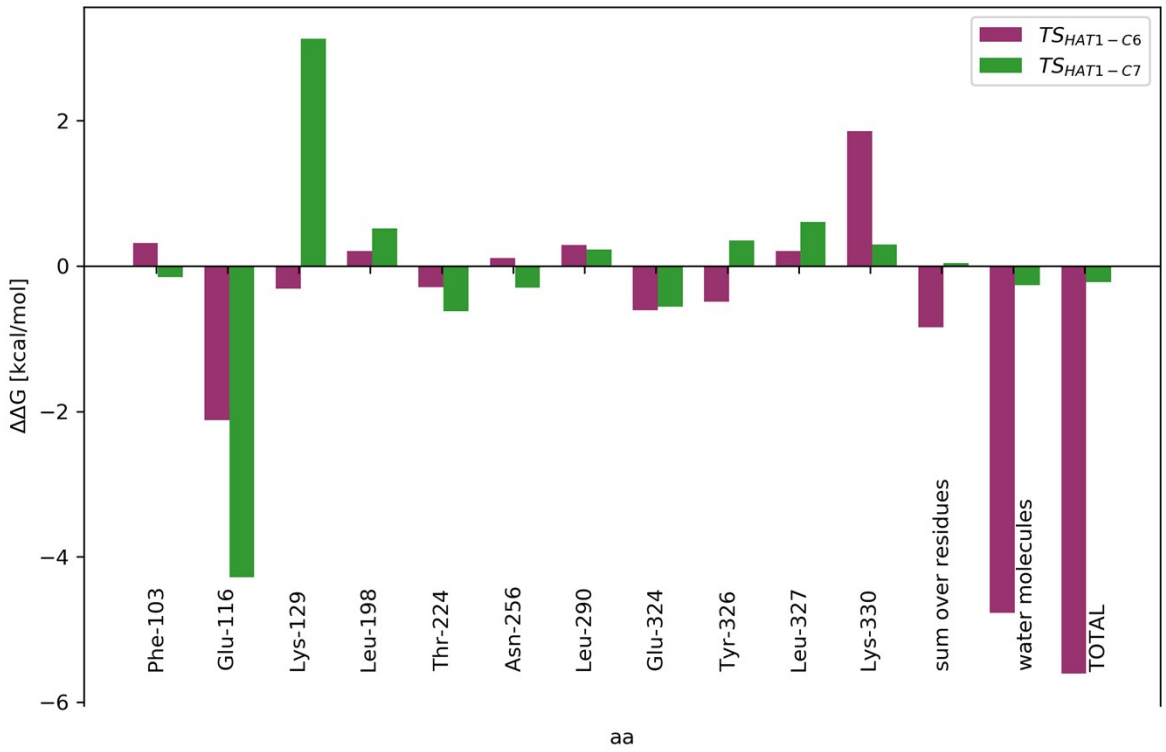

Figure S-C9. Significant (larger than 0.25 kcal mol^{-1}) contributions of the residues' side chains to the relative potential energy barrier (ΔE, calculated at the ONIOM(B3LYP-D3/def2-SVP, Amber) level with mechanical embedding) for $\mathbf{TS_{HAT1-C6}}$ and $\mathbf{TS_{HAT1-C7}}$.

Table S-C2. The ONIOM energy barriers (ΔE) for tH6H variants of $\mathbf{TS_{OH\text{-}C6}}$ and $\mathbf{TS_{OH\text{-}C7}}$ lacking single amino acid side chains. The change in barrier caused by the removal of the side chain is given as ΔΔE. Coulomb, van der Waals and bonded contributions are reported as $\Delta\Delta E^{Coulomb}$, $\Delta\Delta E^{vdW}$ and $\Delta\Delta E^{bond}$, respectively. Values are given in kcal mol^{-1}.

	$TS_{OH\text{-}C6}$					$TS_{OH\text{-}C7}$				
residue	ΔE	ΔΔE	$\Delta\Delta E^{Coulomb}$	$\Delta\Delta E^{vdW}$	$\Delta\Delta E^{bond}$	ΔE	ΔΔE	$\Delta\Delta E^{Coulomb}$	$\Delta\Delta E^{vdW}$	$\Delta\Delta E^{bond}$
none (wt)	7.84					16.59				
Phe-103	7.42	0.42	0.26	0.18	-0.02	16.81	-0.22	-0.39	0.20	-0.04
Leu-105	7.77	0.07	0.05	0.02	0.00	16.50	0.09	0.03	0.06	0.00
Leu-107	7.65	0.18	0.06	0.12	0.01	16.36	0.23	0.06	0.14	0.03
Glu-116	9.16	-1.32	-1.84	0.67	-0.15	24.09	-7.50	-8.28	0.67	0.11
Lys-129	7.30	0.54	0.26	0.15	0.12	7.18	9.41	9.46	0.06	-0.11
Thr-131	7.85	-0.01	-0.08	0.06	0.00	15.39	1.20	0.72	0.62	-0.14
Ala-133	7.61	0.23	0.01	0.17	0.05	16.28	0.30	0.02	0.27	0.01
Ile-194	7.86	-0.02	0.02	0.00	-0.04	16.60	-0.01	0.04	0.00	-0.04
Met-196	7.76	0.08	0.07	-0.03	0.04	16.38	0.21	0.26	0.12	-0.16
Leu-198	7.37	0.46	0.00	0.48	-0.02	15.68	0.91	0.20	0.72	0.00
Asn-200	7.72	0.12	0.03	0.13	-0.04	14.95	1.63	0.34	1.22	0.08
Tyr-202	7.94	-0.10	-0.29	0.26	-0.08	16.68	-0.09	-0.05	-0.25	0.21
Asn-221	7.79	0.05	-0.22	0.30	-0.03	16.44	0.15	-0.01	0.22	-0.06
Thr-224	8.44	-0.60	-0.92	0.36	-0.04	17.55	-0.96	-1.25	0.22	0.06
Leu-226	7.76	0.07	-0.04	0.12	-0.01	16.32	0.27	0.04	**0.24**	0.00
Leu-233	7.98	-0.14	-0.21	0.13	-0.06	16.68	-0.09	-0.14	0.00	0.05
Asn-256	7.97	-0.13	0.02	-0.25	0.10	17.18	-0.59	-0.64	0.18	-0.13
Thr-260	7.91	-0.08	-0.28	0.17	0.04	16.69	-0.11	-0.44	0.27	0.06
Val-276	7.66	0.18	-0.03	0.22	-0.01	16.16	0.43	0.14	**0.31**	-0.03
Leu-290	7.38	0.45	0.04	0.44	-0.02	15.59	0.99	0.16	**0.76**	0.07
Tyr-295	7.74	0.10	0.18	-0.08	0.00	16.49	0.10	0.29	-0.19	0.00
Tyr-319	7.88	-0.04	-0.07	-0.01	0.04	16.72	-0.13	-0.15	0.00	0.02
Ala-320	7.84	0.00	0.00	0.00	0.00	16.59	0.00	0.00	0.00	0.00
Phe-322	7.79	0.05	0.12	-0.06	-0.01	16.56	0.03	0.17	-0.14	0.00
Ala-323	7.89	-0.05	-0.01	-0.05	0.00	16.61	-0.02	0.00	-0.02	0.00
Glu-324	8.46	-0.62	-0.63	0.01	0.00	16.95	-0.36	-0.35	0.00	0.00
Tyr-326	8.29	-0.46	-0.67	0.16	0.06	15.64	0.94	-0.59	1.66	-0.12
Leu-327	7.53	0.31	0.16	0.12	0.04	15.79	0.80	0.05	0.75	0.00
Lys-330	5.20	2.64	2.76	-0.10	-0.02	16.62	-0.03	0.04	-0.04	-0.03
WAT-365	7.56	0.28	0.17	0.12	-0.01	15.79	0.80	0.51	0.30	-0.02
WAT-370	8.76	-0.92	-0.89	-0.05	0.01	16.87	-0.28	-0.29	0.01	0.00
WAT-372	7.72	0.12	0.13	0.00	-0.01	16.44	0.15	0.15	0.01	-0.01
WAT-375	8.75	-0.91	-1.75	0.77	0.08	17.50	-0.91	-4.06	2.94	0.21
WAT-442	7.70	0.14	0.15	-0.01	0.00	16.40	0.19	0.33	-0.14	0.00
WAT-605	7.91	-0.07	0.57	-0.64	-0.01	18.00	-1.41	-0.18	-1.24	0.01
water-1	8.69	-0.85	-1.84	0.88	0.12	19.86	-3.27	-5.58	2.02	0.29

WAT-782	8.04	-0.20	-0.19	-0.02	0.01	16.48	0.11	0.22	-0.10	-0.01
WAT-2175	7.54	0.30	0.51	-0.19	-0.01	16.17	0.42	0.66	-0.22	-0.02
WAT-3097	7.65	0.19	0.29	-0.07	-0.03	15.48	1.10	2.32	-1.11	-0.11
WAT-3155	7.86	-0.03	0.06	-0.09	0.00	16.59	0.00	0.17	-0.16	-0.01
WAT-4290	7.84	0.00	0.01	-0.01	0.00	16.21	0.37	0.51	-0.10	-0.03
WAT-4432	7.60	0.24	0.32	-0.05	-0.02	16.49	0.10	0.15	-0.03	-0.02
WAT-4451	7.59	0.25	0.49	-0.22	-0.03	16.24	0.35	0.56	-0.19	-0.02
WAT-4521	7.84	0.00	0.00	-0.01	0.00	16.71	-0.12	-0.10	-0.02	0.00
WAT-5452	7.83	0.01	0.17	-0.16	-0.01	16.91	-0.32	-0.27	-0.06	0.02
WAT-5484	7.81	0.03	0.32	-0.27	-0.02	16.29	0.30	0.32	0.01	-0.03
WAT-5548	7.80	0.04	-0.11	0.13	0.02	15.78	0.81	1.20	-0.32	-0.07
WAT-5765	7.11	0.72	0.97	-0.23	-0.02	16.33	0.26	0.71	-0.36	-0.10
WAT-6529	7.79	0.05	0.10	-0.05	0.00	16.49	0.10	0.12	-0.02	0.00
WAT-7051	9.00	-1.16	-1.12	-0.08	0.04	16.52	0.07	-0.01	0.08	0.00
WAT-7395	8.95	-1.11	-0.56	-0.58	0.03	16.92	-0.33	-0.59	0.25	0.01
WAT-8073	8.13	-0.29	-0.26	-0.07	0.03	16.19	0.40	0.64	-0.20	-0.04
WAT-9161	8.55	-0.71	-0.54	-0.13	-0.04	14.66	1.93	4.62	-2.39	-0.29
WAT-9453	7.81	0.02	-0.55	0.54	0.03	16.37	0.22	-0.43	0.62	0.03
WAT-9464	7.51	0.33	0.21	0.13	-0.01	16.81	-0.22	-0.38	0.15	0.00
WAT-9501	8.13	-0.29	-0.09	-0.21	0.01	16.48	0.11	0.35	-0.23	0.00
WAT-9665	7.65	0.19	0.59	-0.38	-0.02	16.34	0.25	0.90	-0.63	-0.03
WAT-11739	8.05	-0.22	-0.04	-0.18	0.00	16.50	0.09	0.04	0.05	-0.01
WAT-12117	7.85	-0.02	-0.02	0.00	0.00	16.60	-0.01	-0.01	0.00	0.00
sum over AA		2.38	-1.27	3.7	-0.04		7.6	-0.26	8.04	-0.17
sum over waters		-3.88	-2.89	-1.11	0.12		1.26	2.59	-1.09	-0.24
TOTAL		-1.51	-4.17	2.58	0.08		8.86	2.33	6.95	-0.41

Hydroxylation/desaturation selectivity

In the optimised structure for the radical intermediate **RI_{C6}** the C6 atom hosting the unpaired electron is positioned 3.04 Å from the O atom of the Fe(III)-OH moiety. Such a geometry can facilitate the radical rebound. The *exo* H atom of the neighbouring C7 is located 3.00 Å from the OH group, which suggests that desaturation could also be feasible. Therefore, it might be worthwhile to investigate these two possible fates of the reaction and pinpoint the factors that bias the reaction towards the experimentally observed hydroxylated product (6-hydroxyhyoscyamine).

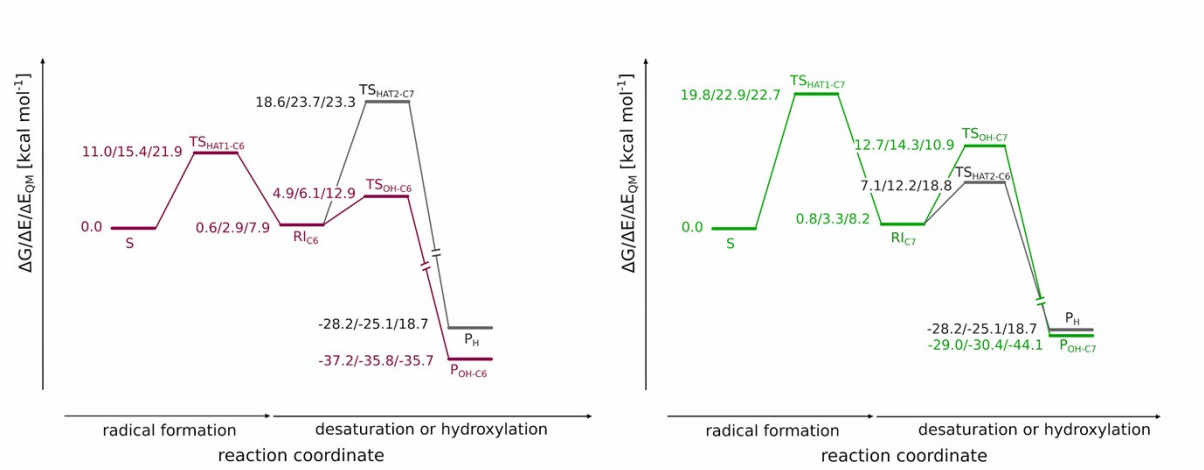

Figure S-C10. Reaction energy profile for tH6H-catalysed hydroxylation and hypothetical desaturation initiated at the C6 (A) and C7 position (B). The energy values, i.e. Gibbs free energy (ΔG), relative potential energy (ΔE) calculated at the ONIOM(B3LYP-D3/def2-TZVP, Amber) level with electronic embedding and the relative potential energy of the QM part (ΔE_{QM}) obtained with the B3LYP-D3/def2-TZVP method (mechanical embedding) are given in kcal mol^{-1}.

The transition state associated with radical rebound (**TS_{OH-C6}**) lies ca. 14 kcal mol^{-1} lower in ΔG than a respective TS for desaturation (**$TS_{HAT2-C7}$**, refer to **Figure S-C10**). The difference in barrier heights is similar when QM energies calculated with mechanical embedding are considered (however the difference in relative electronic energies is slightly smaller. i.e. 10 kcal mol^{-1}). The reaction is driven towards hydroxylation by electronic properties of the reactants as demonstrated by calculations for a cluster model for the active site of tH6H and the substrate molecule. In such a system the barrier for radical rebound process is by 2.4 kcal mol^{-1} lower than the one for second hydrogen abstraction and is close to the electronic energy barrier obtained within the QM/MM scheme (4.7 kcal mol^{-1} with respect to **RI_{C6}** in the cluster model vs 5.0 kcal mol^{-1} in the QM/MM system with mechanical embedding).

The electronic factors that determine hydroxylation/desaturation selectivity were investigated using valence bond theory, which was previously successfully employed for this kind of bifurcation [8]. According to this theory, the energy barrier for the reaction stems from crossing of the reactant and product diabatic potential energy surfaces and its height depends on the excitation energy (promotion gap, G) in the reactant geometry.

The promotion gap of the rebound process (G_{OH}) depends on the strength of the C-O bond that is formed in the reaction and the excitation energy within the Fe(III)-OH complex (E_{Fe}).

$$G_{OH} = BDE_{C-O} + E_{Fe}$$

For the desaturation reaction the gap (G_{HAT}) is determined by the bond dissociation energies (BDE) of the broken C-H and the created H-O on the active site as well as π-bond energy for the unpaired electrons of the neighbouring C atoms and Fe(III)-OH excitation (E_{Fe}):

$$G_{HAT} = BDE_{O-H} + E_{\pi} - BDE_{C-H} + E_{Fe}$$

Thus, the preference towards hydroxylation or desaturation can be decided by the strength of the bonds formed (broken) in the reactions:

$$G_{OH} - G_{HAT} = BDE_{C-O} - (BDE_{O-H} + E_{\pi} - BDE_{C-H})$$

The calculated bond dissociation energy for C6-O, $BDE_{C6\text{-}O}$, totals to 87.7 kcal mol^{-1} and the BDE for C7-H (cleaved during desaturation) is 44.3 kcal mol^{-1}. This value is calculated as the difference between the energy of the unsaturated product and sum of energies of the radical and hydrogen atom, therefore it already includes the π-bond energy as the π-bond is formed simultaneously with the second C-H cleavage. The $BDE_{O\text{-}H}$ for the Fe(II)-OH2 in the active site of H6H is 79.0 kcal mol^{-1}. Therefore, for the C6-centered radical the calculated G_{OH}-G_{HAT} difference is 53.1 kcal mol^{-1}, which indicates an inherent preference of the reactants towards hydroxylation.

Taking into account interactions within the binding pocket reveals that the OH-rebound reaction proceeding at the C6 position is facilitated (by 6.7 kcal mol^{-1}) by the surroundings, whereas the desaturation involving the C7 atom is somewhat destabilised (by 0.4 kcal mol^{-1}). It is consistent with the C6/C7 regioselectivity during HAT described above and the rationale for this effect is also similar. In the optimised structure of **$TS_{OH\text{-}C6}$** the C6-O distance totals to 2.19 Å and the substrate hardly shifts its position to promote contact between C6 atom and OH moiety (see **Figure C1(C)**), such a geometry is stabilised mostly by electrostatic interactions with Glu-116 and surrounding water molecules (as shown in **Figure S-C11(A)** and **C3(A)**). On the other hand, in the optimised structure for **$TS_{HAT2\text{-}C7}$** making close contact between the C7-bound H atom and the OH moiety (1.33 Å, as presented in **Figure S-C12 (A)**) requires a shift of the tropane ring, which leads to unfavourable van der Waals interactions with the adjacent Tyr-326 and destabilising electrostatic interactions with Lys-129 and water molecules (see **Figure S-C11(B)** and **C3(A)**).

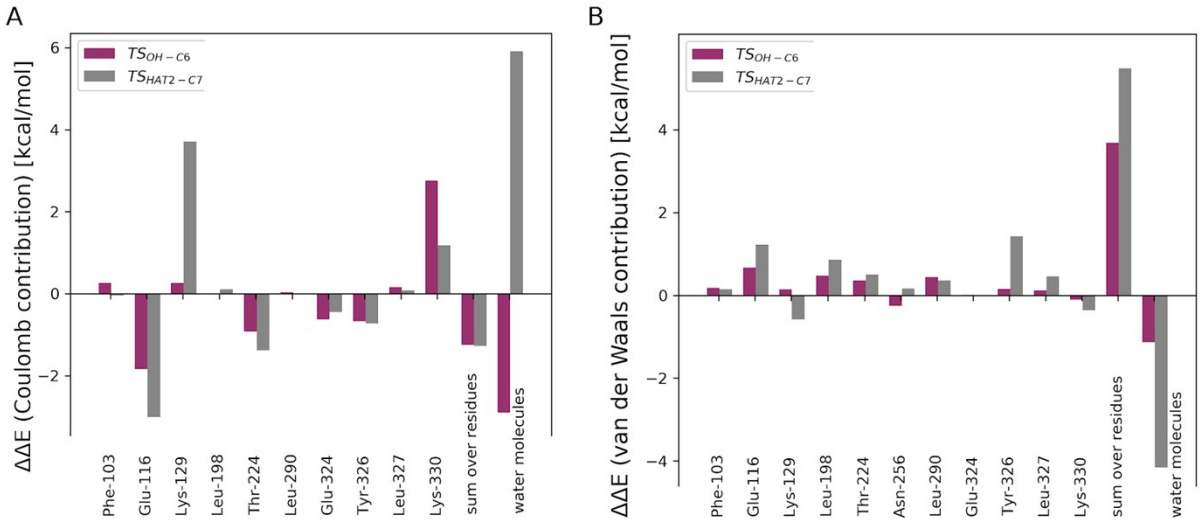

Figure S-C11. The Coulomb (A) and van der Waals (B) contributions of the significant residues' side chains (as shown in **Figure C3 (A)**) to the relative potential energy barrier (ΔE, calculated at the ONIOM(B3LYP-D3/def2-SVP, Amber) level with mechanical embedding) for $\mathbf{TS_{OH\text{-}C6}}$ and $\mathbf{TS_{HAT2\text{-}C7}}$.

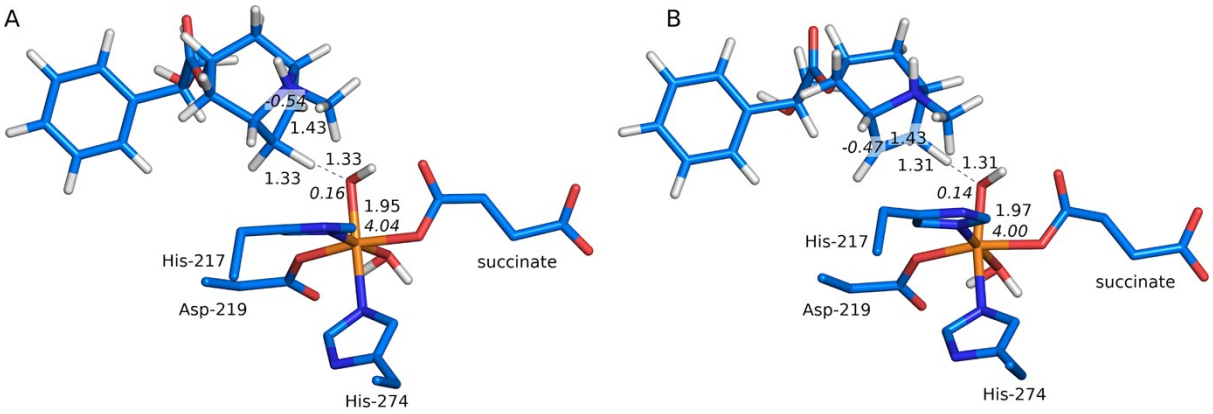

Figure S-C12. QM/MM optimised structures for $\mathbf{TS_{HAT2\text{-}C7}}$ (A) and $\mathbf{TS_{HAT2\text{-}C6}}$ (B). Distances are given in Å and spin populations of absolute value larger than 0.1 are given in italics. Figure rendered with PyMOL [9]; for clarity only the QM region and the MM carboxylate of succinate is shown.

In like manner, for the C7-centered radical the electronic properties of the reactants drive the reaction towards hydroxylation as revealed by analysis based on the VB theory. More specifically, BDE-E_{π} for C7-H totals to 44.7 kcal mol^{-1} and BDE for C7-O is 89.9 kcal mol^{-1}, respectively, and G_{OH}-G_{HAT} equals to 55.6 kcal mol^{-1}, which indicates preference towards hydroxylation. The B3LYP-D3/def2-TZVP energy barrier (computed with mechanical embedding) for the QM system also favours the hydroxylation reaction (10.9 vs 18.8 kcal mol^{-1} for $\mathbf{TS_{OH\text{-}C7}}$ and $\mathbf{TS_{HAT2\text{-}C6}}$, respectively).

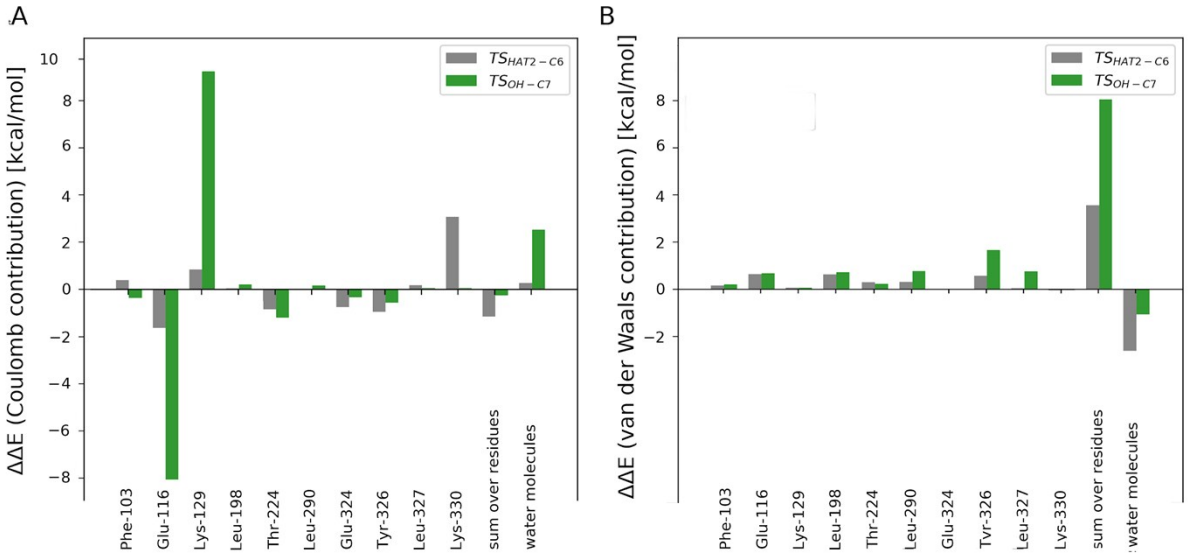

Figure S-C13. Coulomb (A) and van der Waals (B) contributions of the residues' side chains to the relative potential energy barrier (ΔE, calculated at the ONIOM(B3LYP-D3/def2-SVP, Amber) level with mechanical embedding) for **$TS_{HAT2-C6}$** and **TS_{OH-C7}**.

Only taking into account interactions of the QM region with the protein changes the picture and switches the preference towards desaturation. The effect can be assigned to interactions between the substrate molecule and Lys-129/water molecules (electrostatic) as well as with Tyr-326 (van der Waals) that favour reaction occurring at the C6 position, which, in this case, is desaturation (consult **Figures S-C13, S-C15**). A desaturated product has not been observed in experiments, contrary to the C7 hydroxylated one. Indeed, formation of the former cannot be expected, as it is hindered by a relatively high barrier associated with the preceding HAT at the C7 position. The presence of the C7 hydroxylated product may be attributed to some mobility of the substrate within the binding cavity that would (occasionally) facilitate reactions occurring at the C7 position. How this alternative E-S structure might look like is currently not known, yet it is envisioned that starting from it both HAT and subsequent radical rebound at C7 would be the kinetically preferred reactions.

Table S-C3. The ONIOM energy barriers (ΔE) for tH6H variants of **TS_{OH-C6}** and **$TS_{HAT2-C7}$** lacking single amino acid side chains. The change in barrier caused by the removal of the side chain is given as ΔΔE. Coulomb, van der Waals and bonded contributions are reported as $\Delta\Delta E^{Coulomb}$, $\Delta\Delta E^{vdW}$ and $\Delta\Delta E^{bond}$, respectively. Values are given in kcal mol^{-1}.

	TS_{OH-C6}					**$TS_{HAT2-C7}$**				
residue	ΔE	ΔΔE	$\Delta\Delta E^{Coulomb}$	$\Delta\Delta E^{vdW}$	$\Delta\Delta E^{bond}$	ΔE	ΔΔE	$\Delta\Delta E^{Coulomb}$	$\Delta\Delta E^{vdW}$	$\Delta\Delta E^{bond}$
none (wt)	7.84					27.51				
Phe-103	7.42	0.42	0.26	0.18	-0.02	27.43	0.09	-0.04	0.15	-0.02
Leu-105	7.77	0.07	0.05	0.02	0.00	27.42	0.09	0.03	0.06	0.00
Leu-107	7.65	0.18	0.06	0.12	0.01	27.44	0.07	0.05	0.00	0.02
Glu-116	9.16	-1.32	-1.84	0.67	-0.15	29.62	-2.10	-3.01	1.22	-0.32
Lys-129	7.30	0.54	0.26	0.15	0.12	24.21	3.31	3.71	-0.58	0.17

Thr-131	7.85	-0.01	-0.08	0.06	0.00	27.65	-0.14	-0.15	0.01	0.00
Ala-133	7.61	0.23	0.01	0.17	0.05	27.19	0.33	0.00	0.26	0.06
Ile-194	7.86	-0.02	0.02	0.00	-0.04	27.50	0.02	0.02	0.02	-0.03
Met-196	7.76	0.08	0.07	-0.03	0.04	27.36	0.16	0.17	0.06	-0.07
Leu-198	7.37	0.46	0.00	0.48	-0.02	26.61	0.91	0.11	0.86	-0.07
Asn-200	7.72	0.12	0.03	0.13	-0.04	27.12	0.39	0.43	0.00	-0.04
Tyr-202	7.94	-0.10	-0.29	0.26	-0.08	27.56	-0.05	-0.27	0.21	0.02
Asn-221	7.79	0.05	-0.22	0.30	-0.03	27.31	0.20	0.06	0.18	-0.04
Thr-224	8.44	-0.60	-0.92	0.36	-0.04	28.36	-0.84	-1.38	0.50	0.04
Leu-226	7.76	0.07	-0.04	0.12	-0.01	27.40	0.12	0.00	0.11	0.00
Leu-233	7.98	-0.14	-0.21	0.13	-0.06	27.61	-0.10	-0.14	0.06	-0.02
Asn-256	7.97	-0.13	0.02	-0.25	0.10	28.30	-0.79	-0.74	0.17	-0.22
Thr-260	7.91	-0.08	-0.28	0.17	0.04	27.64	-0.12	-0.38	0.21	0.05
Val-276	7.66	0.18	-0.03	0.22	-0.01	27.20	0.31	0.00	0.32	-0.01
Leu-290	7.38	0.45	0.04	0.44	-0.02	27.14	0.38	-0.01	0.36	0.02
Tyr-295	7.74	0.10	0.18	-0.08	0.00	27.47	0.05	0.12	-0.07	0.00
Tyr-319	7.88	-0.04	-0.07	-0.01	0.04	27.58	-0.06	-0.04	-0.04	0.01
Ala-320	7.84	0.00	0.00	0.00	0.00	27.51	0.00	0.00	0.00	0.00
Phe-322	7.79	0.05	0.12	-0.06	-0.01	27.47	0.04	0.11	-0.08	0.01
Ala-323	7.89	-0.05	-0.01	-0.05	0.00	27.54	-0.02	0.00	-0.02	0.00
Glu-324	8.46	-0.62	-0.63	0.01	0.00	27.98	-0.46	-0.45	-0.01	0.00
Tyr-326	8.29	-0.46	-0.67	0.16	0.06	26.95	0.56	-0.73	1.43	-0.14
Leu-327	7.53	0.31	0.16	0.12	0.04	27.00	0.52	0.08	0.46	-0.02
Lys-330	5.20	2.64	2.76	-0.10	-0.02	26.69	0.82	1.18	-0.36	0.00
WAT-365	7.56	0.28	0.17	0.12	-0.01	27.15	0.37	0.12	0.26	-0.01
WAT-370	8.76	-0.92	-0.89	-0.05	0.01	27.83	-0.31	-0.46	0.13	0.02
WAT-372	7.72	0.12	0.13	0.00	-0.01	27.41	0.10	0.11	0.00	-0.01
WAT-375	8.75	-0.91	-1.75	0.77	0.08	28.11	-0.60	-1.01	0.35	0.06
WAT-442	7.70	0.14	0.15	-0.01	0.00	27.43	0.08	0.08	0.00	0.00
WAT-605	7.91	-0.07	0.57	-0.64	-0.01	27.93	-0.42	0.50	-0.90	-0.01
water-1	8.69	-0.85	-1.84	0.88	0.12	26.48	1.03	1.99	-0.90	-0.05
WAT-782	8.04	-0.20	-0.19	-0.02	0.01	27.34	0.17	0.17	0.02	-0.01
WAT-2175	7.54	0.30	0.51	-0.19	-0.01	27.09	0.42	0.55	-0.10	-0.02
WAT-3097	7.65	0.19	0.29	-0.07	-0.03	27.27	0.24	0.91	-0.60	-0.08
WAT-3155	7.86	-0.03	0.06	-0.09	0.00	27.58	-0.07	0.18	-0.24	-0.01
WAT-4290	7.84	0.00	0.01	-0.01	0.00	27.46	0.06	0.10	-0.04	0.00
WAT-4432	7.60	0.24	0.32	-0.05	-0.02	27.39	0.12	0.40	-0.26	-0.02
WAT-4451	7.59	0.25	0.49	-0.22	-0.03	27.40	0.12	0.19	-0.06	-0.01
WAT-4521	7.84	0.00	0.00	-0.01	0.00	27.58	-0.07	-0.09	0.02	0.00
WAT-5452	7.83	0.01	0.17	-0.16	-0.01	27.64	-0.12	0.03	-0.16	0.00
WAT-5484	7.81	0.03	0.32	-0.27	-0.02	27.34	0.17	0.64	-0.45	-0.02
WAT-5548	7.80	0.04	-0.11	0.13	0.02	26.87	0.64	0.72	-0.05	-0.03
WAT-5765	7.11	0.72	0.97	-0.23	-0.02	27.27	0.24	0.18	0.08	-0.02
WAT-6529	7.79	0.05	0.10	-0.05	0.00	27.44	0.07	0.04	0.04	0.00
WAT-7051	9.00	-1.16	-1.12	-0.08	0.04	28.06	-0.55	-0.52	-0.05	0.03

WAT-7395	8.95	-1.11	-0.56	-0.58	0.03	28.21	-0.70	-0.28	-0.44	0.02
WAT-8073	8.13	-0.29	-0.26	-0.07	0.03	27.38	0.13	0.36	-0.22	-0.01
WAT-9161	8.55	-0.71	-0.54	-0.13	-0.04	27.42	0.09	1.40	-1.16	-0.14
WAT-9453	7.81	0.02	-0.55	0.54	0.03	27.50	0.01	-0.87	0.83	0.05
WAT-9464	7.51	0.33	0.21	0.13	-0.01	27.67	-0.15	-0.66	0.49	0.01
WAT-9501	8.13	-0.29	-0.09	-0.21	0.01	27.38	0.14	0.37	-0.23	0.00
WAT-9665	7.65	0.19	0.59	-0.38	-0.02	27.18	0.33	0.58	-0.23	-0.02
WAT-11739	8.05	-0.22	-0.04	-0.18	0.00	27.58	-0.07	0.19	-0.25	-0.01
WAT-12117	7.85	-0.02	-0.02	0.00	0.00	27.52	-0.01	-0.01	0.00	0.00
sum over AA		2.38	-1.27	3.7	-0.04		3.67	-1.23	5.5	-0.6
sum over waters		-3.88	-2.89	-1.11	0.12		1.47	5.89	-4.13	-0.3
TOTAL		-1.51	-4.17	2.58	0.08		5.14	4.66	1.38	-0.89

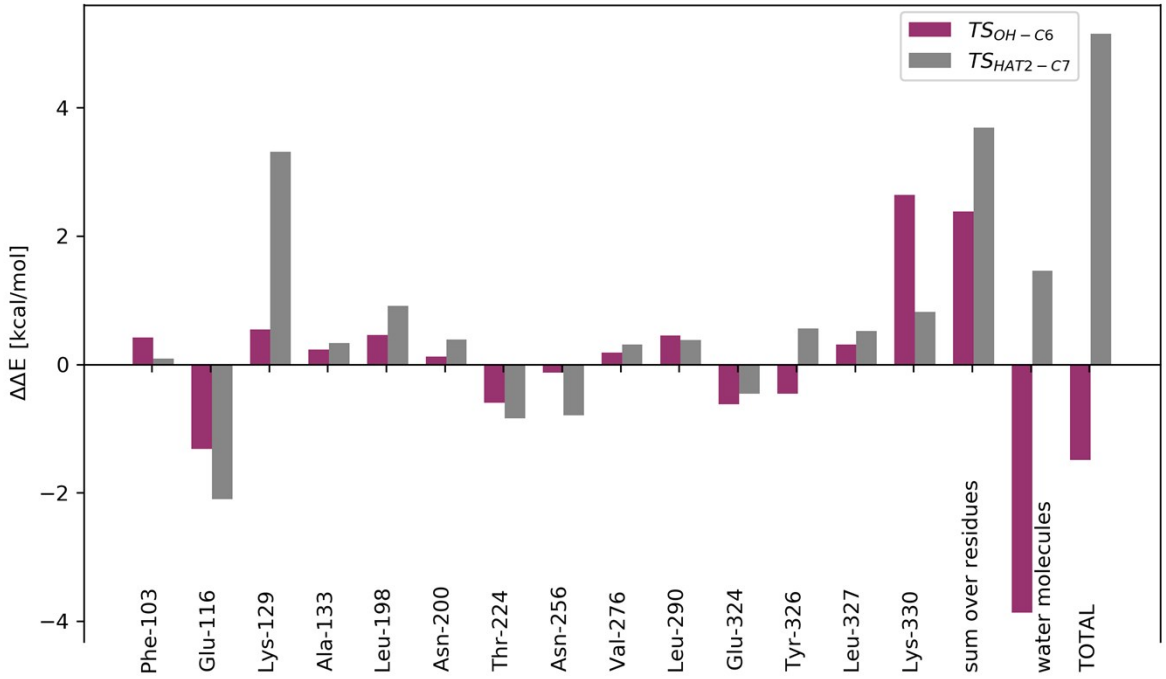

Figure S-C14. Significant (larger than 0.25 kcal mol^{-1}) contributions of the residues' side chains to the relative potential energy barrier (ΔE, calculated at the ONIOM(B3LYP-D3/def2-SVP, Amber) level with mechanical embedding) for $\mathbf{TS_{OH\text{-}C6}}$ and $\mathbf{TS_{HAT2\text{-}C7}}$.

Table S-C4. The ONIOM energy barriers (ΔE) for tH6H variants of $\mathbf{TS_{OH\text{-}C7}}$ and $\mathbf{TS_{HAT2\text{-}C6}}$ lacking single amino acid side chains. The change in barrier caused by the removal of the side chain is given as ΔΔE. Coulomb, van der Waals and bonded contributions are reported as $\Delta\Delta E^{Coulomb}$, $\Delta\Delta E^{vdW}$ and $\Delta\Delta E^{bond}$, respectively. Values are given in kcal mol^{-1}.

residue	ΔE	ΔΔE	$\Delta\Delta E^{Coulomb}$	$\Delta\Delta E^{vdW}$	$\Delta\Delta E^{bond}$	ΔE	ΔΔE	$\Delta\Delta E^{Coulomb}$	$\Delta\Delta E^{vdW}$	$\Delta\Delta E^{bond}$
none (wt)	16.59					13.59				
Phe-103	16.81	-0.22	-0.39	0.20	-0.04	13.00	0.50	0.39	0.15	-0.04
Leu-105	16.50	0.09	0.03	0.06	0.00	13.52	0.07	0.05	0.01	0.00
Leu-107	16.36	0.23	0.06	0.14	0.03	13.45	0.13	0.04	0.09	0.01
Glu-116	24.09	-7.50	-8.28	0.67	0.11	14.84	-1.25	-1.69	0.63	-0.19
Lys-129	7.18	9.41	9.46	0.06	-0.11	12.65	0.94	0.86	0.06	0.02
Thr-131	15.39	1.20	0.72	0.62	-0.14	13.72	-0.14	-0.21	0.07	0.01
Ala-133	16.28	0.30	0.02	0.27	0.01	13.36	0.23	0.00	0.17	0.06
Ile-194	16.60	-0.01	0.04	0.00	-0.04	13.60	-0.02	0.00	0.02	-0.03
Met-196	16.38	0.21	0.26	0.12	-0.16	13.48	0.11	0.03	0.03	0.04
Leu-198	15.68	0.91	0.20	0.72	0.00	12.95	0.63	0.03	0.62	-0.01
Asn-200	14.95	1.63	0.34	1.22	0.08	13.92	-0.34	-0.51	0.20	-0.02
Tyr-202	16.68	-0.09	-0.05	-0.25	0.21	13.52	0.06	0.01	0.01	0.04
Asn-221	16.44	0.15	-0.01	0.22	-0.06	13.59	-0.01	-0.17	0.18	-0.02
Thr-224	17.55	-0.96	-1.25	0.22	0.06	14.18	-0.60	-0.88	0.29	-0.01
Leu-226	16.32	0.27	0.04	**0.24**	0.00	13.61	-0.02	-0.11	0.08	0.00
Leu-233	16.68	-0.09	-0.14	0.00	0.05	13.69	-0.11	-0.19	0.08	0.00
Asn-256	17.18	-0.59	-0.64	0.18	-0.13	13.94	-0.36	-0.25	-0.09	-0.02
Thr-260	16.69	-0.11	-0.44	0.27	0.06	13.69	-0.10	-0.27	0.14	0.03
Val-276	16.16	0.43	0.14	**0.31**	-0.03	13.40	0.18	-0.04	0.23	-0.01
Leu-290	15.59	0.99	0.16	**0.76**	0.07	13.29	0.29	0.00	0.30	-0.01
Tyr-295	16.49	0.10	0.29	-0.19	0.00	13.52	0.07	0.19	-0.12	0.00
Tyr-319	16.72	-0.13	-0.15	0.00	0.02	13.65	-0.07	-0.09	-0.01	0.03
Ala-320	16.59	0.00	0.00	0.00	0.00	13.59	0.00	0.00	0.00	0.00
Phe-322	16.56	0.03	0.17	-0.14	0.00	13.60	-0.02	0.09	-0.10	-0.01
Ala-323	16.61	-0.02	0.00	-0.02	0.00	13.63	-0.04	-0.01	-0.03	0.00
Glu-324	16.95	-0.36	-0.35	0.00	0.00	14.36	-0.78	-0.79	0.01	0.00
Tyr-326	15.64	0.94	-0.59	1.66	-0.12	13.99	-0.40	-0.99	0.56	0.03
Leu-327	15.79	0.80	0.05	0.75	0.00	13.35	0.23	0.17	0.03	0.04
Lys-330	16.62	-0.03	0.04	-0.04	-0.03	10.56	3.02	3.14	-0.05	-0.07
WAT-365	15.79	0.80	0.51	0.30	-0.02	13.29	0.30	0.20	0.11	-0.01
WAT-370	16.87	-0.28	-0.29	0.01	0.00	14.08	-0.49	-0.53	0.02	0.01
WAT-372	16.44	0.15	0.15	0.01	-0.01	13.50	0.08	0.10	-0.01	0.00
WAT-375	17.50	-0.91	-4.06	2.94	0.21	13.94	-0.35	-0.53	0.14	0.04
WAT-442	16.40	0.19	0.33	-0.14	0.00	13.51	0.08	0.07	0.01	0.00
WAT-605	18.00	-1.41	-0.18	-1.24	0.01	13.82	-0.23	0.54	-0.76	-0.02
water-1	19.86	-3.27	-5.58	2.02	0.29	13.12	0.47	-0.12	0.55	0.03
WAT-782	16.48	0.11	0.22	-0.10	-0.01	13.76	-0.17	-0.09	-0.09	0.00

WAT-2175	16.17	0.42	0.66	-0.22	-0.02	13.28	0.31	0.47	-0.15	-0.01
WAT-3097	15.48	1.10	2.32	-1.11	-0.11	13.40	0.19	0.53	-0.29	-0.05
WAT-3155	16.59	0.00	0.17	-0.16	-0.01	13.58	0.00	0.09	-0.08	0.00
WAT-4290	16.21	0.37	0.51	-0.10	-0.03	13.48	0.10	0.14	-0.03	-0.01
WAT-4432	16.49	0.10	0.15	-0.03	-0.02	13.36	0.22	0.43	-0.18	-0.02
WAT-4451	16.24	0.35	0.56	-0.19	-0.02	13.50	0.09	0.19	-0.09	-0.02
WAT-4521	16.71	-0.12	-0.10	-0.02	0.00	13.55	0.04	0.06	-0.02	0.00
WAT-5452	16.91	-0.32	-0.27	-0.06	0.02	13.59	-0.01	0.04	-0.05	0.00
WAT-5484	16.29	0.30	0.32	0.01	-0.03	13.57	0.02	0.23	-0.19	-0.02
WAT-5548	15.78	0.81	1.20	-0.32	-0.07	13.51	0.07	-0.12	0.17	0.02
WAT-5765	16.33	0.26	0.71	-0.36	-0.10	12.75	0.84	1.01	-0.15	-0.02
WAT-6529	16.49	0.10	0.12	-0.02	0.00	13.50	0.09	0.14	-0.05	0.00
WAT-7051	16.52	0.07	-0.01	0.08	0.00	15.08	-1.50	-1.45	-0.11	0.06
WAT-7395	16.92	-0.33	-0.59	0.25	0.01	14.75	-1.17	-0.46	-0.73	0.03
WAT-8073	16.19	0.40	0.64	-0.20	-0.04	13.96	-0.38	-0.31	-0.10	0.03
WAT-9161	14.66	1.93	4.62	-2.39	-0.29	14.50	-0.92	-0.35	-0.53	-0.04
WAT-9453	16.37	0.22	-0.43	0.62	0.03	13.37	0.22	-0.17	0.37	0.01
WAT-9464	16.81	-0.22	-0.38	0.15	0.00	13.32	0.26	0.03	0.24	0.00
WAT-9501	16.48	0.11	0.35	-0.23	0.00	13.87	-0.28	-0.16	-0.13	0.01
WAT-9665	16.34	0.25	0.90	-0.63	-0.03	13.36	0.22	0.65	-0.41	-0.02
WAT-11739	16.50	0.09	0.04	0.05	-0.01	14.01	-0.42	-0.34	-0.08	0.01
WAT-12117	16.60	-0.01	-0.01	0.00	0.00	13.60	-0.02	-0.02	0.00	0.00
sum over AA		7.6	-0.26	8.04	-0.17		2.23	-1.19	3.56	-0.15
sum over waters		1.26	2.59	-1.09	-0.24		-2.35	0.26	-2.60	0
TOTAL		8.86	2.33	6.95	-0.41		-0.12	-0.93	0.96	-0.15

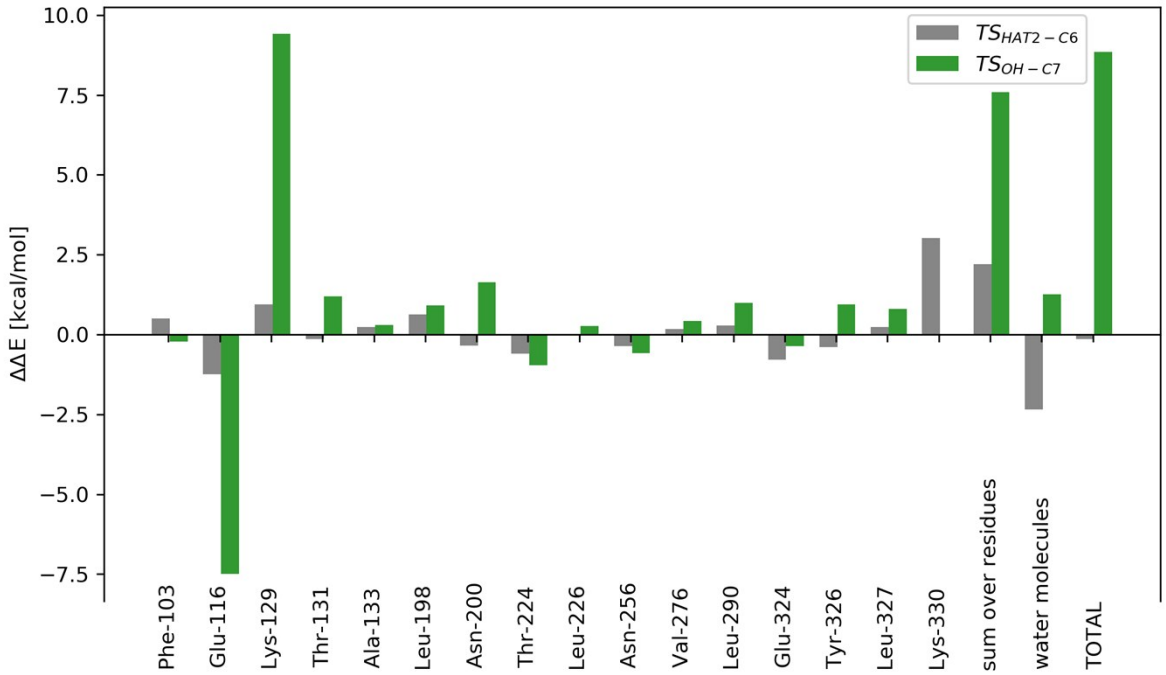

FIgure S-C15. Significant (larger than 0.25 kcal mol^{-1}) contributions of the residues' side chains to the relative potential energy barrier (ΔE, calculated at the ONIOM(B3LYP-D3/def2-SVP, Amber) level with mechanical embedding) for $\mathbf{TS_{HAT2\text{-}C6}}$ and $\mathbf{TS_{OH\text{-}C7}}$.

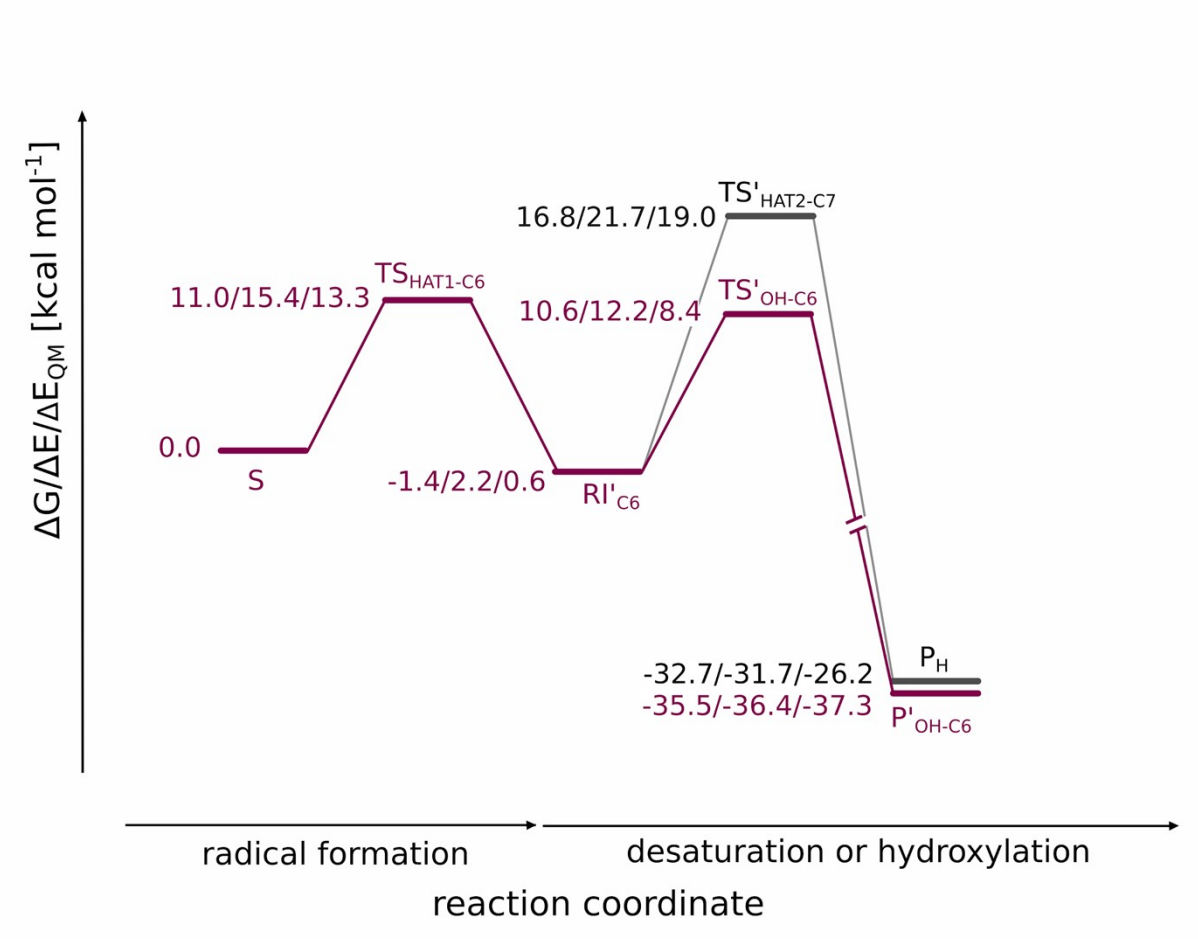

Figure S-C16. Reaction energy profile for tH6H-catalysed hydroxylation and plausible desaturation initiated at the C6 position. The structures of the stationary points lack the Fe(III)-OH---succinate hydrogen bond.

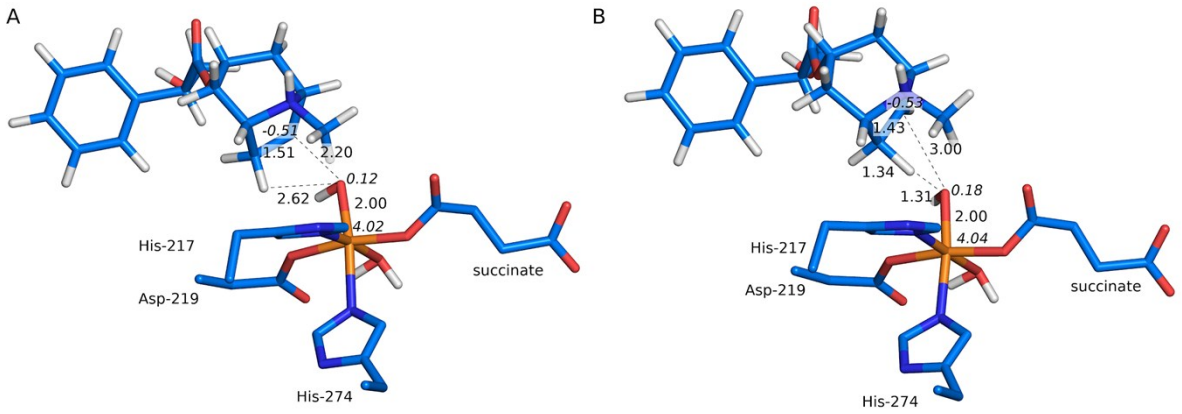

Figure S-C17. Optimised structures for **TS'$_{OH-C6}$** (A) and **TS'$_{HAT2-C7}$** (B). Distances are given in Å and spin populations larger than 0.1 are given in italics.

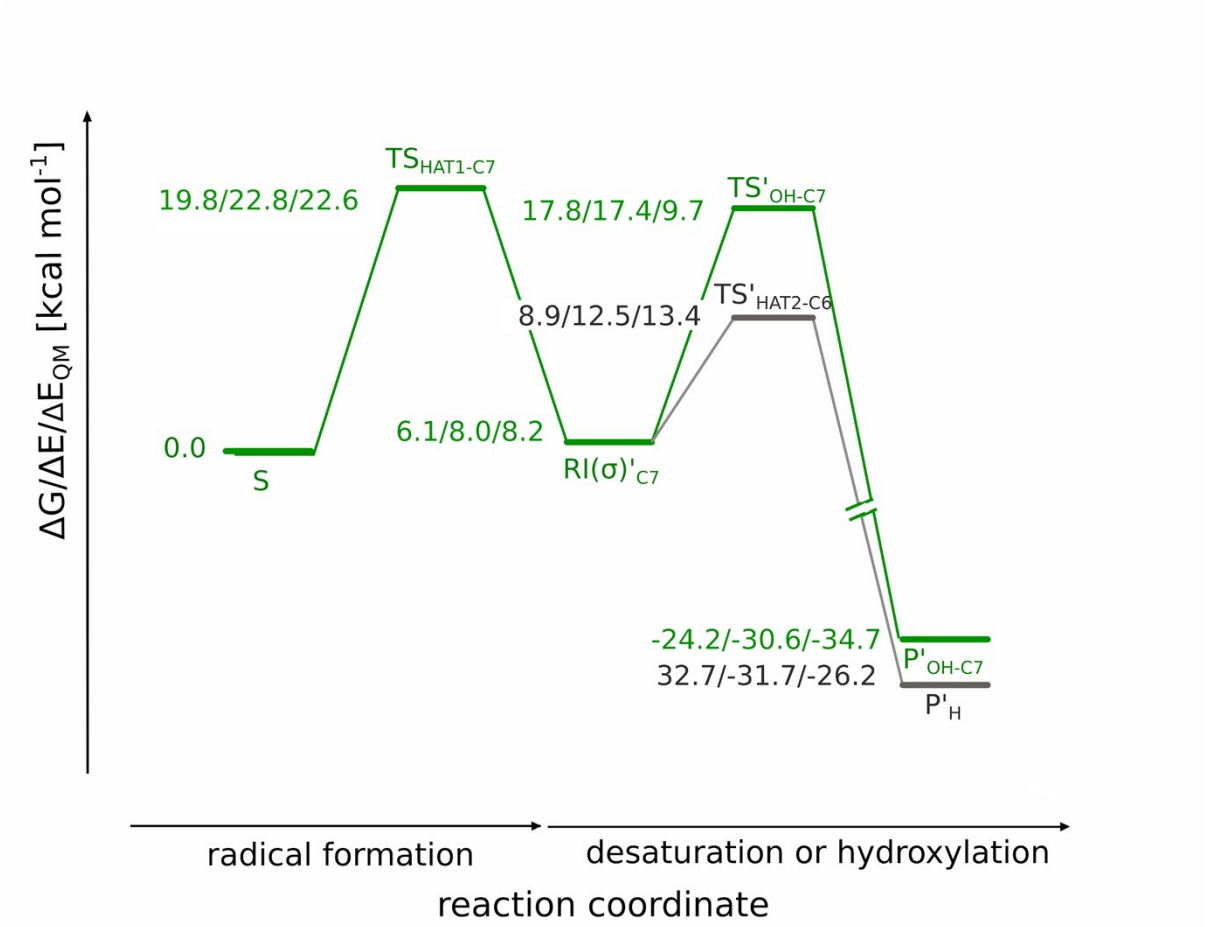

Figure S-C18. Reaction energy profile for tH6H-catalysed hydroxylation and plausible desaturation initiated at the C7 position. The structures of the stationary points lack the -OH---succinate hydrogen bond.

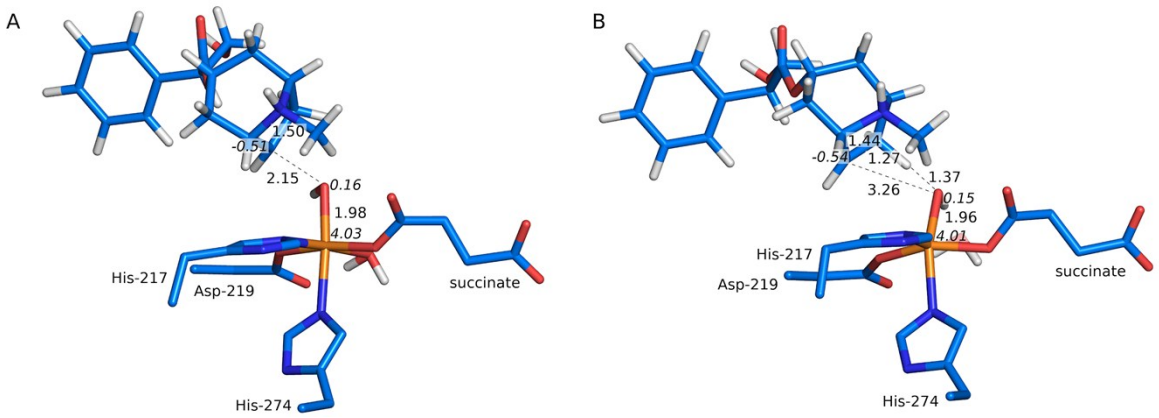

Figure S-C19. Optimised structures for **TS'$_{OH-C7}$** (A) and **TS'$_{HAT2-C6}$** (B). Distances are given in Å and spin populations larger than 0.1 are given in italics.

Table S-C5. Relative energies in kcal mol^{-1} for stationary points in QM/MM calculations; ME stands for mechanical embedding, EE for electronic embedding.

	def2-SVP (ME)		def2-SVP (reopt,ME)		def2-TZVP (ME)		def2-TZVP (EE)		def2-TZVP (EE) water + Lys-129 in QM		**ΔG** def2-TZVP (EE)
	QM	ONIOM	QM	ONIOM	QM	ONIOM	QM	ONIOM	QM	ONIOM	
S'	-1.08	2.45	-0.35	0.01	-0.39	-0.03	2.89	2.22	--	--	**-0.70**
S	0.00	0.00	0.00	0.00	0.00	0.00	0.00	0.00	0.00	0.00	**0.00**
$TS_{HAT1-C6}$	19.49	21.44	21.11	12.62	21.88	13.39	13.32	15.40	14.67	15.31	**11.03**
RI_{C6}	5.55	6.50	7.67	3.31	7.88	3.51	1.86	2.91	2.36	2.95	**0.63**
TS_{OH-C6}	8.22	10.87	11.71	6.67	12.87	7.84	4.42	6.14	5.64	6.82	**4.92**
P_{OH-C6}	-34.04	-40.68	-37.84	-35.43	-35.72	-33.31	-29.55	-35.84	--	--	**-37.21**
$TS_{HAT2-C7}$	18.83	26.63	21.42	25.62	23.32	27.51	22.90	23.74	24.35	25.07	**18.58**
P_H	-19.37	-20.25	-17.44	-22.47	-18.73	-23.76	-28.08	-25.13	--	--	**-28.23**
RI'_{C6}	5.15	7.28	7.54	-2.49	7.78	-2.24	0.55	2.18	--	--	**-1.35**
TS'_{OH-C6}	9.46	11.90	15.94	5.41	17.21	6.68	8.42	12.19	--	--	**10.58**
P'_{OH-C6}	-42.21	-44.82	-33.16	-44.63	-30.87	-42.34	-37.25	-36.42	--	--	**-35.47**
$TS'_{HAT2-C7}$	17.69	24.32	21.00	18.16	22.94	20.10	18.98	21.67	--	--	**16.76**
P'_H	-21.66	-26.56	-21.02	-27.42	-21.93	-28.33	-25.49	-25.79	--	--	**-28.26**
$TS_{HAT1-C7}$ S(Fe)=5/2	20.71	29.68	21.91	23.26	22.67	24.03	19.09	22.85	19.33	24.25	**19.84**
$TS'_{HAT1-C7}$ S(Fe)=3/2	25.15	33.32	25.81	28.66	27.40	30.25	26.38	29.76	26.49	30.15	**26.81**
$RI_{C7}(\pi)$ S(Fe)=3/2	21.13	20.94	22.82	18.95	23.58	19.70	18.74	19.47	19.37	19.96	**17.07**
RI_{C7} S(Fe)=5/2	6.16	7.39	7.74	4.03	8.16	4.45	2.38	3.25	3.49	3.72	**0.75**
TS_{OH-C7}	10.98	24.28	10.07	15.78	10.88	16.59	10.86	14.31	11.05	15.27	**12.73**
P_{OH-C6}	-49.04	-31.71	-49.30	-28.00	-44.13	-22.83	-37.55	-30.41	-39.77	-29.90	**-28.98**
$TS_{HAT2-C6}$	15.24	16.48	17.04	11.79	18.83	13.59	10.95	12.27	13.07	13.75	**7.13**
P_H	-19.29	-20.31	-17.40	-22.63	-18.67	-23.89	-28.09	-25.11	--	--	**-28.18**
$RI'_{C7}(\pi)$			16.32	7.16	17.08	7.91	14.33	13.34	--	--	**11.01**
$RI'_{C7}(\sigma)$	7.09	10.33	6.99	2.62	7.10	2.74	8.17	7.95	--	--	**6.12**
TS'_{OH-C7}	7.79	19.81	12.61	13.10	13.75	14.24	9.70	17.35	--	--	**17.75**
P'_{OH-C6}	-44.56	-36.57	-41.11	-33.62	-38.35	-30.87	-34.74	-30.62	--	--	**-24.17**
$TS'_{HAT2-C6}$	17.21	18.42	24.93	7.72	25.14	7.94	13.43	12.52	--	--	**8.94**
P'_H	-20.86	-30.66	-17.50	-34.56	-18.05	-35.11	-26.16	-31.74	--	--	**-32.67**

References

[1] D.T. Cromer, Calculation of anomalous scattering factors at arbitrary wavelengths, J. Appl. Crystallogr. 16 (1983) 437–437. https://doi.org/10.1107/S0021889883010791.

[2] M.D. Winn, C.C. Ballard, K.D. Cowtan, E.J. Dodson, P. Emsley, P.R. Evans, R.M. Keegan, E.B. Krissinel, A.G.W. Leslie, A. McCoy, S.J. McNicholas, G.N. Murshudov, N.S. Pannu, E.A. Potterton, H.R. Powell, R.J. Read, A. Vagin, K.S. Wilson, Overview of the CCP 4 suite and current developments, Acta Crystallogr. D Biol. Crystallogr. 67 (2011) 235–242. https://doi.org/10.1107/S0907444910045749.

[3] E.R. Johnson, S. Keinan, P. Mori-Sánchez, J. Contreras-García, A.J. Cohen, W. Yang, Revealing noncovalent interactions, J. Am. Chem. Soc. 132 (2010) 6498–6506. https://doi.org/10.1021/ja100936w.

[4] J. Contreras-García, E.R. Johnson, S. Keinan, R. Chaudret, J.-P. Piquemal, D.N. Beratan, W. Yang, NCIPLOT: A Program for Plotting Noncovalent Interaction Regions, J. Chem. Theory Comput. 7 (2011) 625–632. https://doi.org/10.1021/ct100641a.

[5] R.C. Wilmouth, J.J. Turnbull, R.W.D. Welford, I.J. Clifton, A.G. Prescott, C.J. Schofield, Structure and Mechanism of Anthocyanidin Synthase from Arabidopsis thaliana, Structure 10 (2002) 93-103. https://doi.org/10.1016/S0969-2126(01)00695-5.

[6] Z. Zhang, J. Ren, D.K. Stammers, J.E. Baldwin, K. Harlos, C.J. Schofield, Structural origins of the selectivity of the trifunctional oxygenase clavaminic acid synthase, Nat. Struct. Biol. 7 (2000) 127-133. https://doi.org/10.1038/72398.

[7] I.J. Clifton, L.X. Doan, M.C. Sleeman, M. Topf, H. Suzuki, R.C. Wilmouth, C.J. Schofield, Crystal Structure of Carbapenem Synthase (CarC), J. Biol. Chem. 278 (2003) 20843-20850. https://doi.org/10.1074/jbc.M213054200.

[8] L. Ji, A.S. Faponle, M.G. Quesne, M.A. Sainna, J. Zhang, A. Franke, D. Kumar, R. van Eldik, W. Liu, S.P. de Visser, Drug Metabolism by Cytochrome P450 Enzymes: What Distinguishes the Pathways Leading to Substrate Hydroxylation Over Desaturation?, Chem. - A Eur. J. 21 (2015) 9083–9092. https://doi.org/10.1002/chem.201500329.

[9] The PyMOL Molecular Graphics System, Version 1.8, Schrödinger LLC, 2015.